

Supporting Information

Exploiting Trifluoromethyl Substituents for Tuning Orbital Character of Singlet and Triplet States to Increase the Rate of Thermally Activated Delayed Fluorescence

Jonathan S. Ward, Andrew Danos, Patrycja Stachelek, Mark A. Fox, Andrei S. Batsanov, Andrew P. Monkman^{}, Martin R. Bryce^{*}*

Table of Contents

S1 General Synthetic Chemistry Experimental Details	2
S2 Synthetic procedures.....	3
S3 ¹ H and ¹³ C{ ¹ H} NMR spectra	11
S4 Solution Electrochemical Analysis.....	23
S5 Photophysical and optoelectronic data.....	24
S6 X-ray Crystallographic data.....	31
S7 Computational data.....	35
S8 References	44

S1 General Synthetic Chemistry Experimental Details

All reactions were carried out under an argon atmosphere unless otherwise stated. Starting materials were purchased commercially and were used as received. Solvents were dried using an Innovative Technology solvent purification system and were stored in ampoules under argon.

TLC analysis was carried out using Merck Silica gel 60 F₂₅₄ TLC plates and spots were visualized using a TLC lamp emitting at 365 or 254 nm. Silica gel column chromatography was performed using Silica Gel 60 purchased from Fluorochem.

¹H, ¹⁹F and ¹³C{¹H} NMR spectroscopy was carried out on Bruker AV400, Varian VNMRs 600 and 700 spectrometers. Residual solvent peaks were referenced as described in the literature,¹ and all NMR data were processed in MestReNova V12. Due to broadening of some ¹³C NMR peaks by coupling to neighbouring ¹⁹F nuclei, the full expected multiplicity of some ¹³C peaks was not observed in all cases.

High resolution mass spectrometry was carried out on a Waters LCT Premier XE using ASAP ionization with TOF detection. Samples were analyzed directly as solids. All reference to Br within characterization data refers to ⁷⁹Br isotope.

Melting points were performed on a Stuart SMP40 machine with a ramping rate of 4 °C min⁻¹ and are uncorrected.

Any stated use of hexane refers to a mix isomers grade.

Molecule **1** was compared using a literature sample already synthesized and reported.²

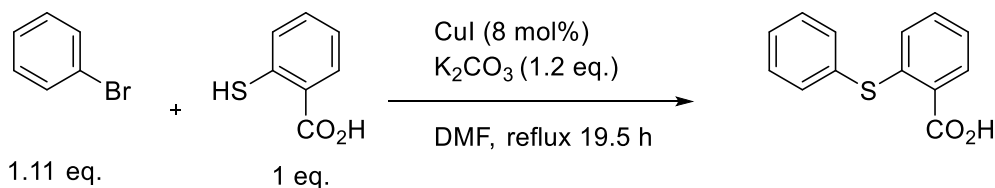
9,9-dimethyl-9,10-dihydroacridine (**19**) was synthesized using literature procedures.³

2,7-dibromo-9,9-dimethylthioxanthene S,S-dioxide (**20**) was synthesized using literature procedures⁴

3,6-dimethoxycarbazole (**21**) was synthesized using literature procedures.⁵

2 Synthetic procedures

2-(phenylthio)benzoic acid (**7**)

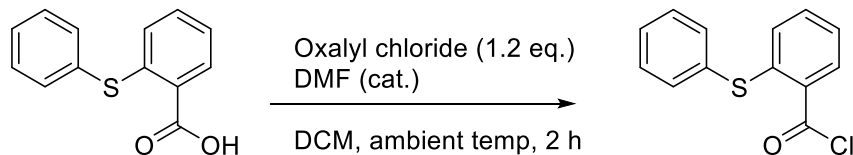


This molecule was synthesized using a literature procedure but with an improved workup procedure to aid with the removal of copper impurities.⁶ Data is consistent with the literature.⁶

Bromobenzene (7.00 g, 4.68 ml, 44.5 mmol, 1.11 eq.) was added to a suspension of thiosalicylic acid **6** (6.14 g, 39.8 mmol, 1 eq.), K₂CO₃ (6.66 g, 48 mmol, 1.2 eq.) and copper iodide (600 mg, 3.15 mmol, 7.8 mol%) in DMF (75 ml). The reaction mixture was refluxed under argon for 19.5 h and filtered through a pad of celite at room temperature. The filtrate was diluted with water (500 mL) and acidified with 10% HCl (30 mL) until a colorless solid precipitated. Copper impurities were removed from the mixture by addition of EtOAc (300 mL) and washing the organic layer with 1 M citric acid (2 × 100 mL) and 1 M HCl (2 × 100 mL). The organic layer was dried with MgSO₄ and filtered. Removal of solvent under reduced pressure yielded product as a white solid (2.41 g, 26%).

¹H NMR (400 MHz, DMSO-*d*₆) δ 13.21 (s, 1H), 7.91 (dd, *J* = 7.6, 1.5 Hz, 1H), 7.57 – 7.47 (m, 5H), 7.36 (ddd, *J* = 8.2, 7.6, 1.5 Hz, 1H), 7.21 (td, *J* = 7.6, 1.2 Hz, 1H), 6.72 (dd, *J* = 8.2, 1.2 Hz, 1H).

2-(phenylthio)benzoyl chloride (**8**)

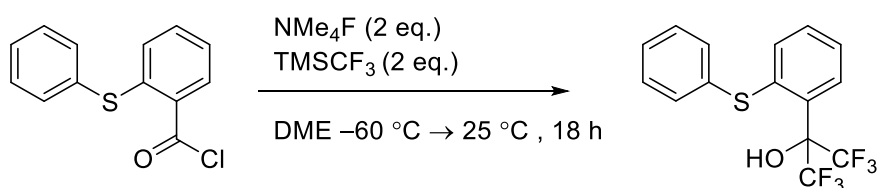


This molecule is known, but this synthesis was based on a modified literature procedure of a different molecule.⁷ Data is consistent with the literature.⁷

To a solution of 2-(phenylthio)benzoic acid (**7**) (2.24 g, 9.73 mmol, 1 eq.) in dry dichloromethane (20 mL) under argon was added oxalyl chloride (987 μL, 1.48 g, 11.66 mmol, 1.2 eq.) dropwise. Following this dry DMF (3 drops) was added and the reaction was stirred at ambient temperature for 2 h. The solvent was removed under reduced pressure and the product was obtained and used without further purification (2.25 g, 93%).

¹H NMR (400 MHz, CDCl₃) δ 8.31 (dd, *J* = 8.0, 1.5 Hz, 1H), 7.60 – 7.53 (m, 2H), 7.51 – 7.43 (m, 3H), 7.33 (ddd, *J* = 8.2, 7.3, 1.5 Hz, 1H), 7.22 (ddd, *J* = 8.0, 7.3, 1.2 Hz, 1H), 6.83 (dd, *J* = 8.2, 1.2 Hz, 1H).

1,1,1,3,3,3-hexafluoro-2-(2-(phenylthio)phenyl)propan-2-ol (**9**)

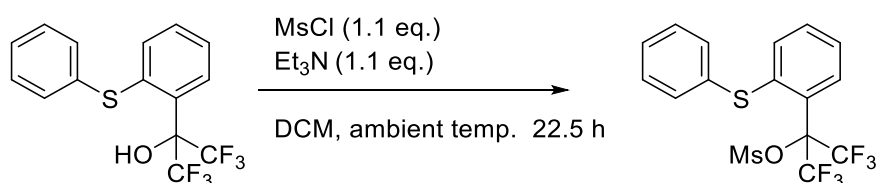


2-(phenylthio)benzoyl chloride (**8**) (2.20 g, 8.84 mmol, 1 eq.) was added to 100 mL a three-necked round-bottomed flask equipped with a stirrer bar and reflux condenser. To a powder addition flask was rapidly added NMe₄F (1.64 g, 17.69 mmol, 2 eq.) which was immediately attached to the side arm of the three-neck flask

(NMe₄F is highly hygroscopic). The set up was immediately evacuated and only the powder addition flask was vigorously heated under vacuum for 5 min to ensure NMe₄F was dry. Following cooling of the powder addition flask and 1 h further drying under vacuum at room temperature, the flask was backfilled with argon. Dry DME (25 mL) was added to the acid chloride *via* cannula and was stirred until dissolution was achieved. The solution was then cooled to -60 °C using a dry ice/acetone bath, then TMSCF₃ (2.61 mL/2.51 g, 17.7 mmol, 2 eq.) was added dropwise followed by portion-wise addition of the NMe₄F in the powder addition flask. The reaction mixture was allowed to warm to -30 °C for 1 h and was then allowed to stir warming to ambient temperature overnight. The reaction mixture was quenched with 2 M HCl (20 mL) and was extracted with Et₂O (2 × 100 mL). The organic extracts were washed with H₂O (2 × 50 mL) and were dried with MgSO₄ and filtered. Removal of solvent under reduced pressure yielded a crude oil. The crude oil was purified with silica gel column chromatography eluting with 10–30% DCM:hexane (*v/v*) by increasing DCM in 10% increments. Removal of solvent under reduced pressure yielded product as a clear oil (2.00 g, 64%).

¹H NMR (700 MHz, Acetone-*d*₆) δ 8.01 (s, 1H), 7.69 – 7.64 (m, 1H), 7.49 – 7.40 (m, 5H), 7.35 – 7.29 (m, 2H), 7.10 (s, 1H); ¹³C NMR (176 MHz, Acetone-*d*₆) δ 140.8, 135.4, 134.9, 133.1, 131.2, 130.7, 129.6, 129.3, 128.6, 126.7, 124.3 (q, *J* = 290 Hz) 81.6 (apr. t, *J* = 29 Hz); ¹⁹F NMR (376 MHz, Acetone-*d*₆) δ -74.2; HRMS-ASAP-TOF⁺ *m/z* calculated for C₁₅H₁₀F₆OS [M]⁺ 352.0351, found: 352.0336.

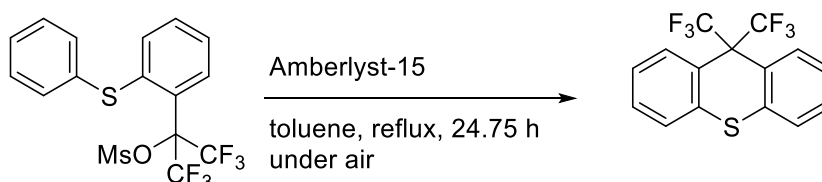
1,1,1,3,3,3-hexafluoro-2-(2-(phenylthio)phenyl)propan-2-yl-methanesulfonate (**10**)



To a solution of 1,1,1,3,3,3-hexafluoro-2-(2-(phenylthio)phenyl)propan-2-ol (**9**) (1.99 g, 5.65 mmol, 1 eq.) in dry DCM (50 mL) under argon was slowly added Et₃N (865 μL/628 mg, 6.21 mmol, 1.1 eq.). The reaction mixture was cooled to 0 °C and MsCl (480 μL/0.71 g, 6.21 mmol, 1.1 eq.) was added dropwise. The reaction was stirred at ambient temperature for 22.5 h. The reaction mixture was quenched with sat. NaHCO_{3(aq)} (20 mL). The aqueous layer was separated and the organic layer was washed with H₂O (2 × 50 mL) followed by brine (50 mL). The organic layer was dried with MgSO₄ and filtered. Removal of solvent under reduced pressure yielded product as a viscous clear oil (2.25 g, 93%).

¹H NMR (700 MHz, Acetone-*d*₆) δ 7.76 – 7.71 (m, 1H), 7.54 – 7.50 (m, 2H), 7.47 – 7.36 (m, 5H), 7.29 – 7.25 (m, 1H), 3.65 (s, 3H); ¹³C NMR (176 MHz, acetone-*d*₆) δ 140.9, 136.0, 134.8, 133.6, 131.9, 130.7, 129.9, 129.3, 127.4, 125.9, 122.7 (q, *J* = 293 Hz), 87.3 (apr. pent, *J* = 31 Hz), 40.1; ¹⁹F NMR (376 MHz, Acetone-*d*₆) δ -68.2; HRMS-ASAP-TOF⁺ *m/z* calculated for C₁₆H₁₂F₆O₃S₂ [M]⁺ 430.0127, found: 430.0132.

9,9-bis(trifluoromethyl)-9H-thioxanthene (**11**)

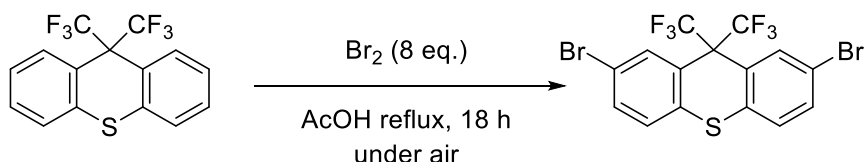


To a solution of mesylate **10** (4.51 g, 10.48 mmol, 1 eq.) in toluene (200 mL) was added Amberlyst-15 (33.5 g, 4.7 mmol ‘-SO₃H’ g⁻¹). The reaction mixture was refluxed with vigorous stirring for 24.75 h. GC-MS analysis confirmed consumption of the starting material and product formation. The reaction mixture was filtered in a glass sinter and the Amberlyst-15 was washed repeatedly with CHCl₃ (7 × 100 mL) with vigorous agitation in the sinter during each wash before suction was applied. The solvent was removed under reduced pressure to yield a crude mixture. The crude mixture was purified by silica gel column chromatography eluting

with hexane followed by 5% DCM:hexane (v/v). Removal of solvent under reduced pressure gave product as a white crystalline solid (2.26 g, 64%).

^1H NMR (700 MHz, Acetone- d_6) δ 8.10 – 8.06 (m, 2H), 7.53 (ddd, $J = 8.0, 7.0, 1.2$ Hz, 2H), 7.49 (ddd, $J = 8.0, 1.7, 0.5$ Hz, 2H), 7.43 (ddd, $J = 8.6, 7.0, 1.7$ Hz, 2H); ^{13}C NMR (176 MHz, acetone) δ 132.8, 132.43 (sept, $J = 5$ Hz), 131.1, 127.34, 127.28, 125.1 (q, $J = 287$ Hz), 121.8, 59.0 (apr. pent. $J = 26$ Hz); ^{19}F NMR (376 MHz, CD_2Cl_2) δ -63.08; HRMS-ASAP-TOF $^+$ m/z calculated for $\text{C}_{15}\text{H}_8\text{F}_6\text{S}$ $[\text{M}]^+$ 334.0245, found:334.0255.

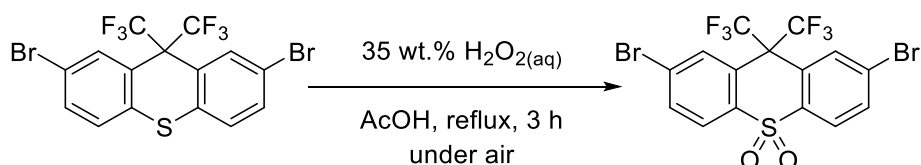
2,7-dibromo-9,9-bis(trifluoromethyl)-9H-thioxanthene (12)



To a stirring solution of 9,9-bis(trifluoromethyl)-9H-thioxanthene (**11**) (1.00 g, 2.99 mmol, 1 eq.) in AcOH (25 L) was added Br_2 (3.82 g, 1.23 mL, 23.92 mmol, 8 eq.) dropwise. The reaction was heated using a Drysyn kit set at 120 °C and was stirred overnight with a reflux condenser fitted. GC-MS(EI $^+$) analysis showed complete conversion after 18 h. The reaction was quenched by pouring into ice water allowing for precipitation of the product. The product was filtered in a glass sinter and was washed copiously with H_2O (5×100 mL). The product was dried in an oven at 70 °C for 1 h and then under vacuum at ambient temperature to give product as a slightly yellow solid (1.36 g, 92%).

^1H NMR (400 MHz, $\text{DCM}-d_2$) δ 8.17 – 8.11 (m, 2H), 7.56 (dd, $J = 8.5, 2.0$ Hz, 2H), 7.25 (d, $J = 8.5$ Hz, 2H); ^{19}F NMR (376 MHz, CD_2Cl_2) δ -63.18; ^{13}C NMR (176 MHz, CD_2Cl_2) δ 134.6 (apr. pent, $J = 5$ Hz), 133.5, 131.3, 128.0, 124.9, 123.2, 122.9, 119.9, 58.5 (apr. pent, $J = 27$ Hz); HRMS-ASAP-TOF $^+$ m/z calculated for $\text{C}_{15}\text{H}_6\text{F}_6\text{SBr}_2$ $[\text{M}]^+$ 489.8456, found:489.8464.

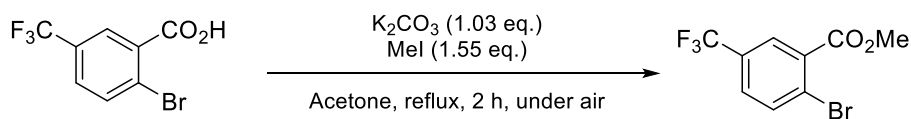
2,7-dibromo-9,9-bis(trifluoromethyl)-9H-thioxanthene-S,S-dioxide (13)



Compound **12** (780 mg, 1.59 mmol, 1 eq.) was dissolved in AcOH (25 mL) and the mixture was heated up to 80 °C with stirring. $\text{H}_2\text{O}_{2(\text{aq})}$ (10 mL, 35 wt.% in H_2O) was then added to the mixture portion-wise. The reaction was then heated to reflux (Drysyn kit set to 120 °C) for 3 h. The reaction was allowed to cool to ambient temperature overnight to allow for precipitation of product. The product was filtered in a glass sinter and was washed with H_2O (5×100 mL) with mixing in the sinter before applying suction during each wash. The white solid obtained was dried in an oven at 70 °C for 1 h and then under vacuum at ambient temperature overnight. The solid was recrystallized from toluene. Filtering of the product and drying overnight under high vacuum yielded product (466 mg, 56%).

^1H NMR (400 MHz, $\text{DCM}-d_2$) δ 8.37 – 8.34 (m, 2H), 8.17 (d, $J = 8.5$ Hz, 2H), 8.02 (dd, $J = 8.5, 1.7$ Hz, 2H); ^{13}C NMR (176 MHz, CD_2Cl_2) δ 136.7, 135.9, 135.0 (sept, $J = 4$ Hz), 128.5, 126.3, 126.0, 123.2 (q, $J = 288$ Hz), 55.9 (apr. pent, $J = 27$ Hz); ^{19}F NMR (376 MHz, CD_2Cl_2) δ -63.10; HRMS-ASAP-TOF $^+$ m/z calculated for $\text{C}_{15}\text{H}_7\text{F}_6\text{O}_2\text{SBr}_2$ $[\text{MH}]^+$ 522.8432, found: 522.8443.

methyl 2-bromo-5-(trifluoromethyl)benzoate (15)

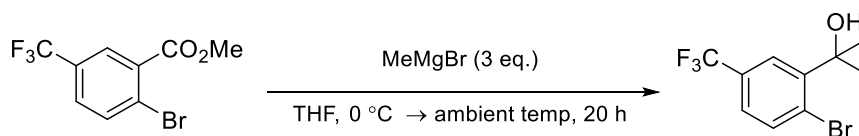


This molecule is known but was made via a modified procedure. Data is consistent with the literature.⁸

To a 500 mL round-bottomed flask was added 2-bromo-5-(trifluoromethyl)benzoic acid (14.80 g, 55.0 mmol, 1 eq.), K_2CO_3 (7.83 g, 56.7 mmol, 1.03 eq.), acetone (200 mL) and MeI (5.3 mL/12.07 g, 85.0 mmol, 1.55 eq.). The flask was fitted with a reflux air condenser and heated to reflux (60 °C Drysyn temp.) for 2 h with stirring. The reaction was allowed to cool to ambient temperature and the acetone was removed under reduced pressure. DCM (200 mL) and water (200 mL) was added to dissolve the residue from the reaction mixture. The organic layer was separated and the aqueous layer was extracted with DCM (2 × 100 mL). All organic extracts were combined, dried with $MgSO_4$ and filtered. Removal of solvent under reduced pressure yielded product as a colourless oil (15.07 g, 97%).

1H NMR (400 MHz, Acetone- d_6) δ 8.11 (d, $J = 2.3$ Hz, 1H), 8.01 (d, $J = 8.4$ Hz, 1H), 7.82 (dd, $J = 8.4, 2.3$ Hz, 1H), 3.95 (s, 3H).

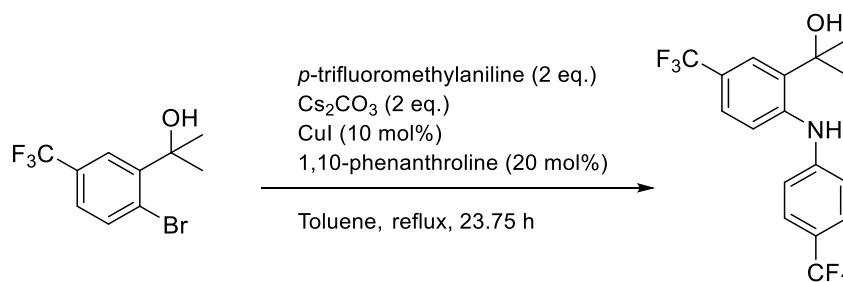
2-(2-bromo-5-(trifluoromethyl)phenyl)propan-2-ol (16)



Methyl 2-bromo-5-(trifluoromethyl)benzoate **15** (14.98 g, 52.9 mmol, 1 eq.) was added to a 250 mL 2-neck round-bottomed flask equipped with a stirrer bar and was dried under vacuum. The flask was backfilled with argon and dry THF (70 mL) was added *via* cannula. The reaction was cooled to 0 °C and MeMgBr [53 mL (3.0 M solution in Et_2O), 159 mmol, 3 eq.] was added dropwise via syringe over 30 min. The reaction mixture was then allowed to warm to ambient temperature and was stirred for 20 h. The reaction was quenched by slow dropwise addition of H_2O to the reaction mixture until fizzing ceased. The reaction mixture was then diluted with EtOAc (100 mL) and transferred to a separating funnel. The reaction flask was washed out with H_2O (100 mL) and transferred to the separating funnel. The organic layer was separated and the aqueous layer was extracted with EtOAc (2 × 100 mL). The organic layers were combined and were washed with brine (200 mL). The organic layer was separated, dried with $MgSO_4$ and filtered. Removal of solvent under reduced pressure gave crude product. The crude product was purified by silica gel column chromatography eluting with gradient EtOAc:hexane (0:1) increasing to (15:85) (v/v). The solvent was removed under reduced pressure to give the product as an off white solid (12.63 g, 84%). Note: This molecule shows some suspected slow rotation about the dimethylmethylene–aryl bond. In combination with 1H - ^{19}F coupling this makes many signals broad and assignment of multiplicity is not universally possible in this system. The hindered rotation has an effect on both the 1H and $^{13}C\{^1H\}$ NMR spectra, where some signals are duplicated in unequal ratios due to the hindered rotation discussed.

1H NMR (400 MHz, Acetone- d_6) δ 8.35 – 8.25 (m, 1H), 7.84 (d, $J = 8.2$ Hz, 1H), 7.53 – 7.44 (m, 1H), 4.67 (s, 1H), 1.77 – 1.73 (m, 6H); ^{13}C NMR (176 MHz, Acetone- d_6) δ 150.5, 136.8, 136.7, 130.0 (q, $J = 32$ Hz), 125.8 (br.), 125.6 (br.), 125.3 (q, $J = 272$ Hz), 124.9, 73.1, 73.0, 29.13, 29.07; ^{19}F NMR (376 MHz, Acetone- d_6) δ –63.23. HRMS-ASAP-TOF⁺ m/z calculated for $C_{10}H_9BrF_3 [M-OH]^+$ 264.9834, found: 264.9841.

2-(5-(trifluoromethyl)-2-((4-(trifluoromethyl)phenyl)amino)phenyl)propan-2-ol (**17**)

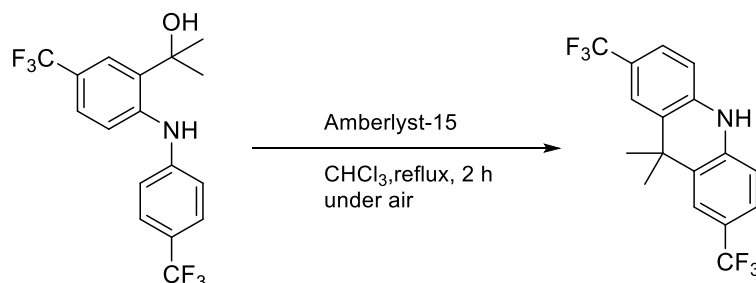


This molecule is new but was prepared using a modified literature procedure.⁹

To a 2-neck round-bottomed flask equipped with a stirrer bar and reflux condenser was added alcohol **16** (4.24 g, 14.9 mmol, 1 eq.), CuI (283 mg, 1.49 mmol, 10 mol%), 1,10-phenanthroline (537 mg, 2.98 mmol, 20 mol%) and Cs₂CO₃ (9.74 g, 29.8 mmol, 2 eq.). The flask was dried under high vacuum for 30 min and the flask was backfilled with argon. Dry toluene (30 mL) was added via syringe, followed by *p*-trifluoromethylaniline (3.76 mL/4.82 g, 29.9 mmol, 2 eq.). The reaction mixture was deoxygenated by bubbling with argon for 30 min. The reaction mixture was refluxed (Drysyn temp 115 °C) for 23.75 h. The reaction was allowed to cool to ambient temperature and water (50 mL) was added followed by EtOAc (100 mL). The organic layer was separated and the aqueous layer was extracted with EtOAc (2 × 100 mL). The organic layers were combined and were dried with MgSO₄ and filtered. Removal of solvent under reduced pressure gave crude product. The crude product was purified by silica gel column chromatography eluting with gradient EtOAc:hexane (1:19) to (1:9) (v/v). The solvent was removed under reduced pressure to give the product as a yellowish crystalline solid (2.56 g, 47%). In combination with ¹H-¹⁹F coupling this makes the signals broad and assignment of multiplicity is not universally possible in this system. The hindered rotation has an effect on both the ¹H and ¹³C{¹H} NMR spectra, where some signals are duplicated in unequal ratios due to the hindered rotation discussed.

¹H NMR (700 MHz, Acetone-*d*₆) δ 9.17 (s, 1H), 7.62 – 7.59 (m, 3H), 7.59 – 7.56 (m, 1H), 7.55 – 7.52 (m, 1H), 7.30 (d, *J* = 8.5 Hz, 2H), 5.25 – 4.98 (m, 1H), 1.70 – 1.69 (m, 6H); ¹⁹F NMR (376 MHz, Acetone-*d*₆) δ –61.9, –62.0; ¹³C NMR (176 MHz, Acetone-*d*₆) δ 147.05, 146.95, 145.63, 145.62, 145.62, 145.49, 137.32, 137.30, 127.63 (q, *J* = 4 Hz), 126.54, 125.8 (q, *J* = 4 Hz), 125.76 (q, *J* = 270 Hz), 124.09 (q, *J* = 4 Hz), 122.65 (q, *J* = 32 Hz), 122.57 (q, *J* = 32 Hz), 119.14, 119.10, 118.00, 117.91, 74.07, 74.04, 29.75; HRMS-ASAP-TOF⁺ *m/z* calculated for C₁₇H₁₆F₆NO [MH]⁺ 364.1131, found: 364.1143;

9,9-dimethyl-2,7-bis(trifluoromethyl)-9,10-dihydroacridine (**18**)

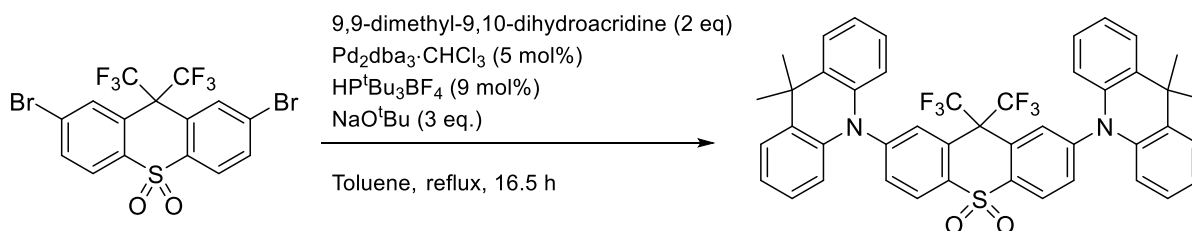


To a solution of diarylamine **17** (2.00 g, 5.50 mmol, 1 eq.) in 70 mL of CHCl₃, was added Amberlyst-15 (11.71 g, 4.7 mmol ‘–SO₃H’ g⁻¹). The reaction mixture was refluxed with vigorous stirring for 2 h. GCMS analysis showed the reaction had gone to completion. The reaction mixture was filtered in a glass sinter and the Amberlyst-15 was washed repeatedly with CHCl₃ (10 × 100 mL) with vigorous agitation in the sinter during each wash before suction was applied. The solvent was removed under reduced pressure to yield a crude mixture. The crude mixture was purified by silica gel column chromatography eluting with hexane followed

by 5% DCM:hexane (*v/v*). Removal of solvent under reduced pressure gave product **18** as a white crystalline solid (1.18 g, 62%).

¹H NMR (700 MHz, Acetone-*d*₆) δ 8.96 (s, 1H), 7.77 – 7.69 (m, 2H), 7.47 – 7.40 (m, 2H), 7.03 (d, *J* = 8.3 Hz, 2H), 1.67 (s, 6H); ¹³C NMR (176 MHz, Acetone-*d*₆) δ 142.0, 141.9, 129.8, 129.7, 126.0 (q, *J* = 270 Hz), 125.2 (q, *J* = 4 Hz), 123.9 (q, *J* = 4 Hz), 123.0 (q, *J* = 32 Hz), 115.1, 115.0, 37.17, 37.16, 31.6, 31.5; ¹⁹F NMR (376 MHz, Acetone-*d*₆) δ -61.7; HRMS-ASAP-TOF⁺ *m/z* calculated for C₁₇H₁₄F₆N [MH]⁺ 346.1025, found: 346.1029;

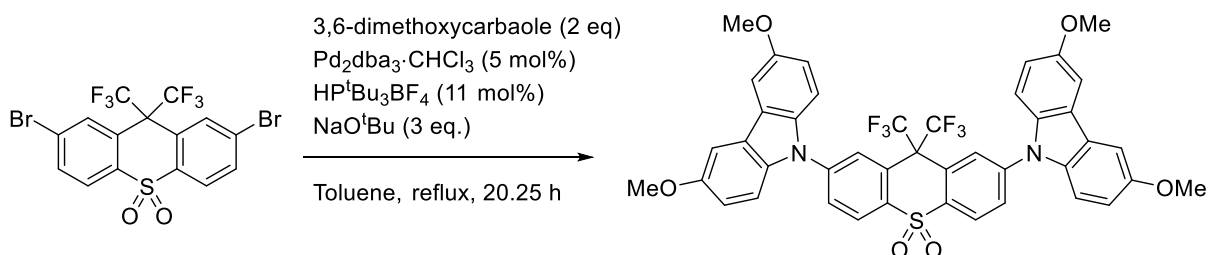
2,7-bis(9,9-dimethylacridin-10-yl)-9,9-bis(trifluoromethyl)-9H-thioxanthene-S,S-dioxide (**2**) – General procedure A



2,7-dibromo-9,9-bis(trifluoromethyl)-9H-thioxanthene-S,S-dioxide (**13**) (212 mg, 0.405 mmol, 1 eq.) and 9,9-dimethyl-9,10-dihydroacridine (**19**) (170 mg, 0.810 mmol, 2 eq.) were dried under vacuum for 30 min in a two-neck 100 mL round bottomed flask fitted with a reflux condenser. The flask was back-filled with argon and dry toluene (10 mL) was added. The reaction mixture was purged with argon for 30 min, then Pd₂(dba)₃·CHCl₃ (21 mg, 20 μmol, 0.05 eq.) and HP^tBu₃BF₄ (11 mg, 38 μmol, 0.09 eq.) were added and the reaction mixture was purged with argon for a further 30 min. NaO^tBu (117 mg, 1.22 mmol, 3 eq.) was added under a high flow of argon and the reaction mixture was heated to 115 °C (Drysyn kit temp.) with stirring for 16.5 h. The reaction was allowed to cool to ambient temperature and was filtered through Celite™, and the celite was washed with DCM until TLC analysis showed all product was washed through. The solvent was removed under reduced pressure and the crude mixture was purified by silica gel column chromatography eluting with gradient DCM:hexane 1:1 to 4:1 (*v/v*). Removal of solvent under reduced pressure produced a crude solid which was suspended in pentane (5 mL) and was sonicated for 30 seconds. Filtration and washing with cold pentane (2 × 10 mL), and drying under high vacuum gave the product as a yellow crystalline solid (230 mg, 73% yield).

¹H NMR (400 MHz, CD₂Cl₂) δ 8.53 (d, *J* = 8.5 Hz, 2H), 8.23 – 8.14 (m, 2H), 7.88 (dd, *J* = 8.5, 1.9 Hz, 2H), 7.57 – 7.47 (m, 4H), 7.12 – 6.98 (m, 8H), 6.49 – 6.40 (m, 4H), 1.67 (s, 12H); ¹³C NMR (176 MHz, CD₂Cl₂) δ 146.9, 140.5, 135.8, 133.5, 132.6 (apr. pent. *J* = 5 Hz), 132.3, 127.8, 127.2, 127.0, 125.9, 123.5 (q, *J* = 288 Hz), 122.8, 116.2, 56.3 (apr. pent *J* = 27 Hz), 36.8, 30.7; ¹⁹F NMR (376 MHz, CD₂Cl₂) δ -63.14; HRMS-ASAP-TOF⁺ *m/z* calculated for C₄₅H₃₅F₆N₂O₂S [MH]⁺ 781.2318, found: 781.2328; m. p.: 259–261 °C.

2,7-bis(3,6-dimethoxycarbazol-N-yl)-9,9-bis(trifluoromethyl)-9H-thioxanthene-S,S-dioxide (**3**)



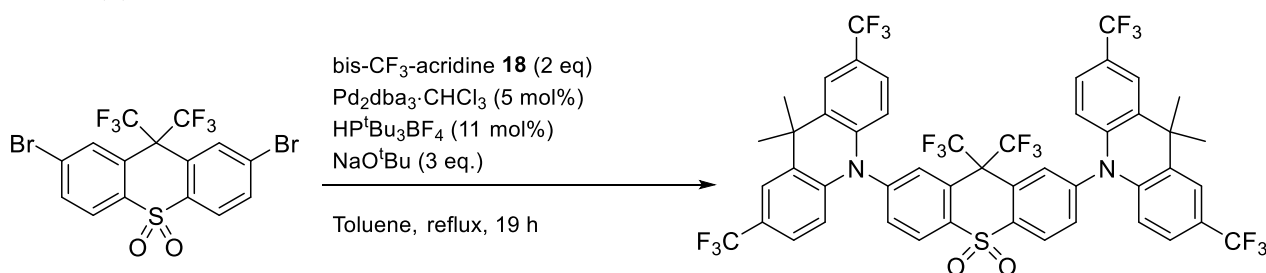
Using general procedure A, **13** (100 mg, 0.1908 mmol, 1 eq.), 3,6-dimethoxycarbazole (**21**) (88 mg, 0.038 mmol, 2 eq), toluene (9 mL), Pd₂(dba)₃·CHCl₃ (10 mg, 10 μmol, 0.05 eq.), HP^tBu₃BF₄ (6 mg, 20 μmol, 0.11 eq.) and NaO^tBu (55 mg, 0.57 mmol, 3 eq.) were used to make the title compound with 20.25 h reaction time. Work up was performed as in general procedure A. Silica gel column chromatography was performed using a

column packed with DCM:hexane:Et₃N (70:30:1) (v/v). The product was loaded and eluted with gradient DCM:hexane (7:3) to 100% DCM. The solvent was removed under reduced pressure and the product was recrystallized from boiling hexane with dropwise addition of DCM until dissolution was achieved. Cooling the mixture to -18 °C resulted in product precipitation which was filtered and washed with cold pentane (2 × 5 mL). Drying the material under high vacuum overnight gave the product as a yellow crystalline solid (105 mg, 67%). Crystals suitable for X-ray diffraction were obtained by layering a solution of **3** in DCM with hexane. Slow mixing of the layers resulted in formation of yellow crystals.

¹H NMR (400 MHz, CD₂Cl₂) δ 8.56 (d, *J* = 8.5 Hz, 2H), 8.46 (br. s, 2H), 8.14 (dd, *J* = 8.5, 1.8 Hz, 2H), 7.60 (d, *J* = 2.5 Hz, 4H), 7.45 (d, *J* = 9.0 Hz, 4H), 7.10 (dd, *J* = 9.0, 2.5 Hz, 4H), 3.95 (s, 12H); ¹³C NMR (176 MHz, CD₂Cl₂) δ 155.5, 143.2, 135.4, 135.0, 129.6, 129.2 (br.), 126.9, 126.7, 125.2, 124.7 (q, *J* = 289 Hz), 115.8, 110.8, 103.7, 56.4. ¹⁹F NMR (376 MHz, CD₂Cl₂) δ -62.8; HRMS-ASAP-TOF⁺ *m/z* calculated for C₄₃H₃₀F₆N₂O₆S [M]⁺ 816.1723, found: 816.1742. m.p.: 333–335 °C.

Note: In the ¹³C NMR spectrum, the signal corresponding to the quarternary carbon substituted with the two trifluoromethyl groups on the thioxanthene-*S,S*-dioxide acceptor unit could not be observed due to splitting of the peaks (expected septet) reducing the signal/noise ratio significantly. This signal was observed in several other cases at 55–60 ppm.

2,7-bis(9,9-dimethyl-2,7-bis(trifluoromethyl)acridin-*N*-yl)-9,9-bis(trifluoromethyl)-9*H*-thioxanthene-*S,S*-dioxide (4**)**

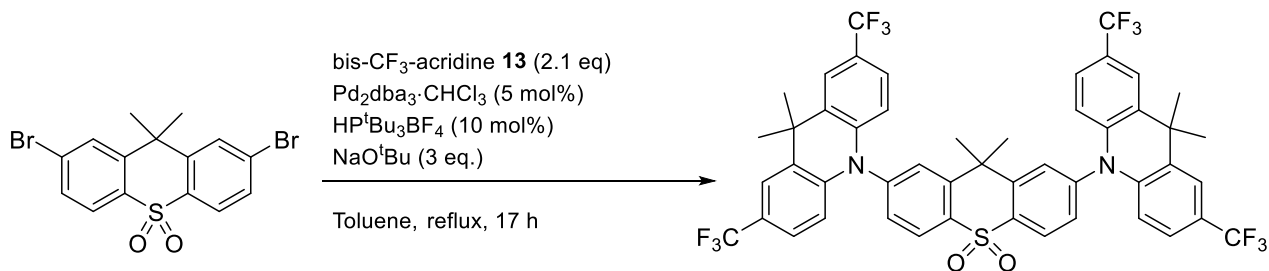


Using general procedure **A**, **13** (100 mg, 0.1908 mmol, 1 eq.), 9,9-dimethyl-2,7-bis(trifluoromethyl)-9,10-dihydroacridine **18** (88 mg, 0.38 mmol, 2 eq), toluene (9 mL), Pd₂(dba)₃·CHCl₃ (10 mg, 10 μmol, 0.05 eq.), HP^tBu₃BF₄ (6 mg, 20 μmol, 0.11 eq.) and NaO^tBu (55 mg, 0.57 mmol, 3 eq.) were used to make the title compound with 19 h reaction time. Work up was performed as in general procedure **A**. Silica gel column chromatography was performed eluting with gradient DCM: hexane (3:7), increasing to 7:3 (v/v). Removal of solvent under reduced pressure yielded a white solid which was sonicated in pentane (5 mL) and filtered in a sinter. The product was washed with cold pentane (2 × 5 mL) and was dried under high vacuum overnight to give product as a white solid (130 mg, 65%). Crystals suitable for X-ray diffraction were obtained by layering a solution of **4** in DCM with hexane. Slow mixing of the layers resulted in formation of clear colorless crystals.

¹H NMR (400 MHz, CD₂Cl₂) δ 8.72 (d, *J* = 8.4 Hz, 2H), 8.21 (br. s, 2H), 7.94 (dd, *J* = 8.4, 1.8 Hz, 2H), 7.77 (d, *J* = 1.7 Hz, 4H), 7.29–7.34 (m, 4H), 6.31 (d, *J* = 8.5 Hz, 4H), 1.76 (s, 12H); ¹³C NMR (176 MHz, CD₂Cl₂) δ 144.9, 142.4, 138.3, 135.53, 135.50, 131.1, 128.8, 127.8, 125.0 (q, *J* = 272 Hz), 124.59 (q, *J* = 4 Hz), 124.56 (q, *J* = 33 Hz), 123.60 (q, *J* = 4 Hz), 114.5, 36.8, 31.6. ¹⁹F NMR (376 MHz, CD₂Cl₂) δ -62.0, -63.0; HRMS-ASAP-TOF⁺ *m/z* calculated for C₄₉H₃₁F₁₈N₂O₂S [MH]⁺ 1053.1813, found: 1053.1838; m. p. : 298–300 °C.

Note: In the ¹³C NMR, the signal corresponding to the trifluoromethyl carbon on the thioxanthene-*S,S*-dioxide acceptor unit could not be observed due to splitting of the peaks reducing the signal/noise significantly. This signal was observed in several other cases at 120–125 ppm, although in general the signal is weak. The X-ray crystal structure confirms the presence of the bis-CF₃ functionality on the acceptor unit.

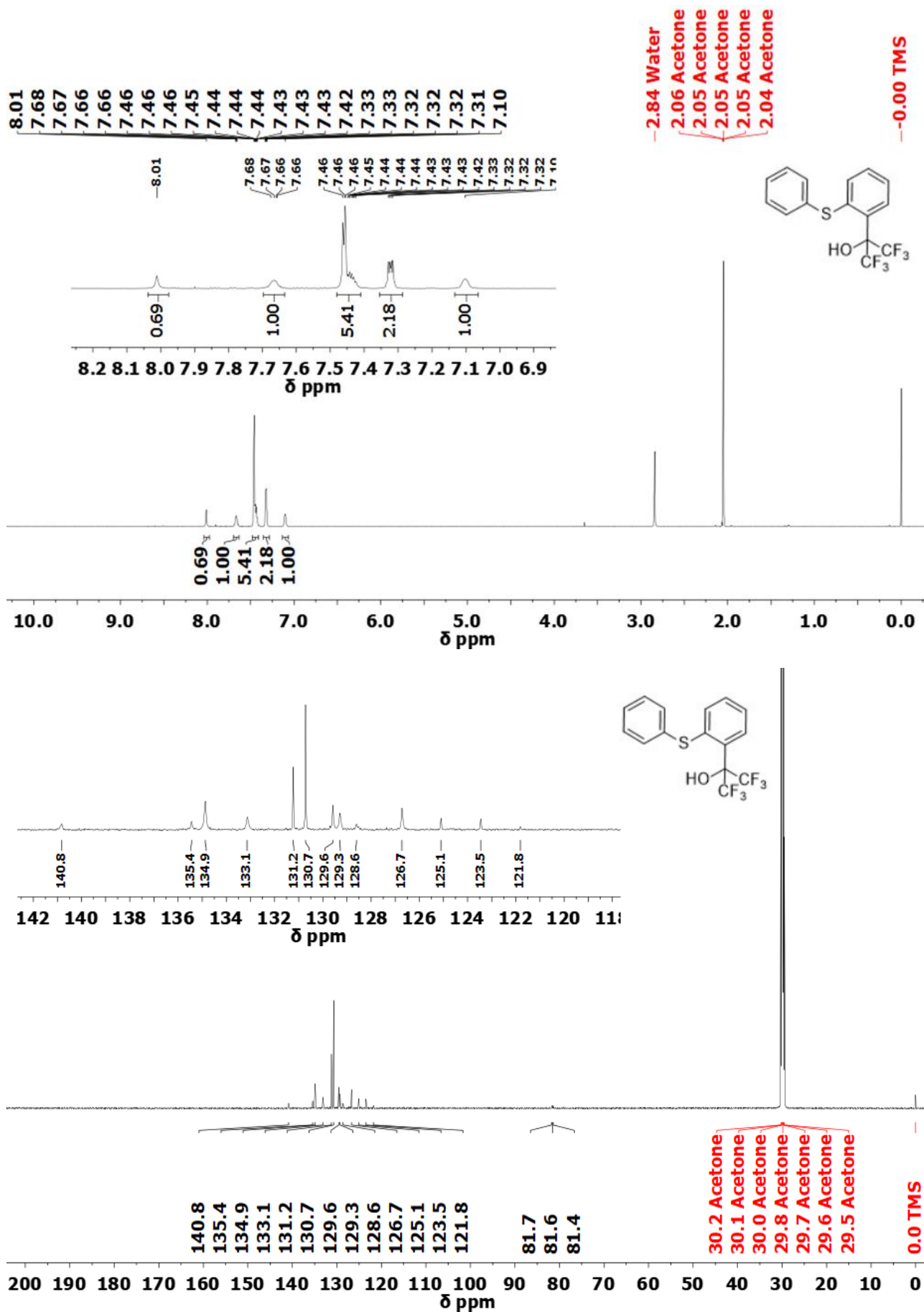
2,7-bis(9,9-dimethyl-2,7-bis(trifluoromethyl)acridin-N-yl)-9,9-dimethyl-9H-thioxanthene-S,S-dioxide (5)

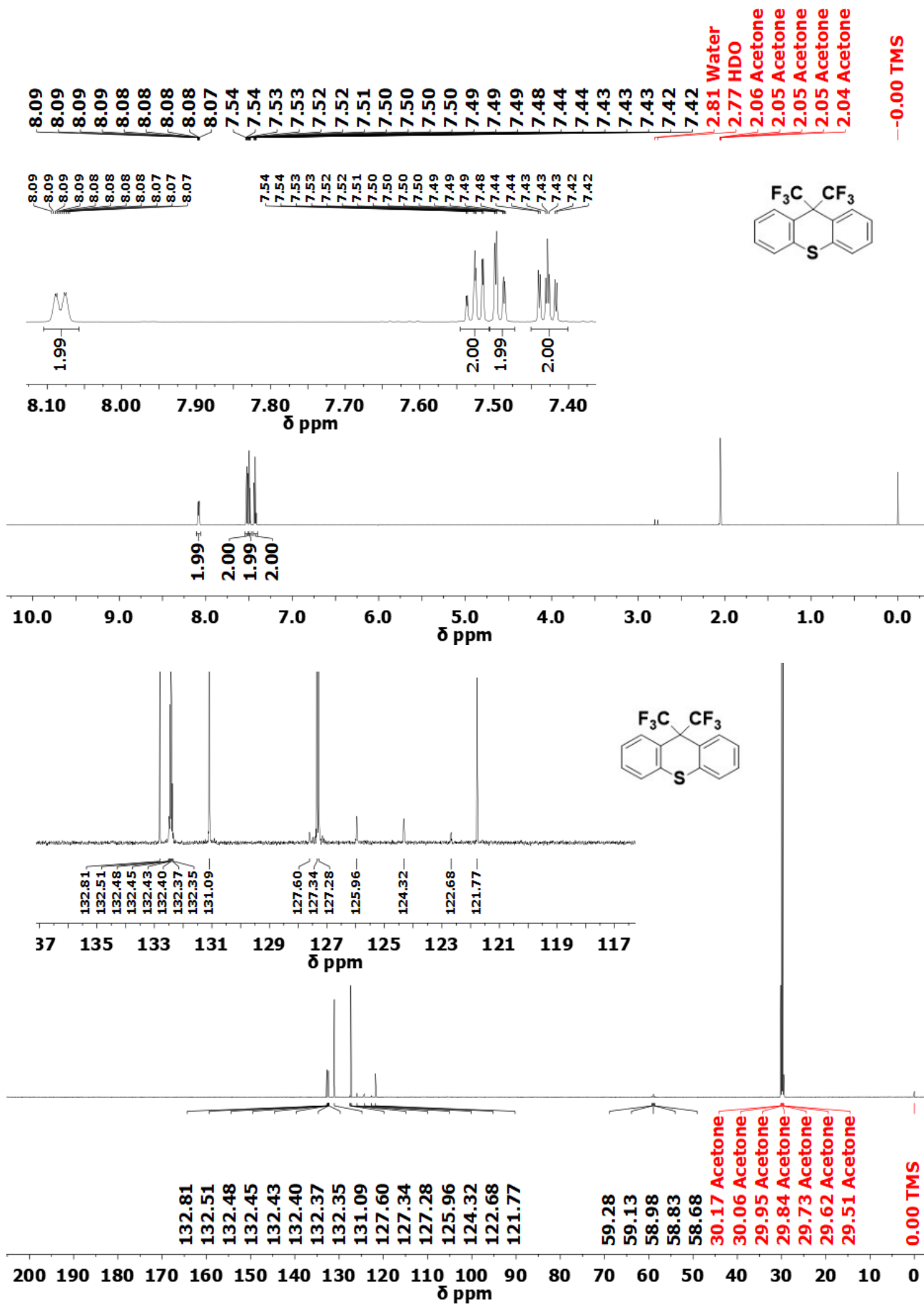


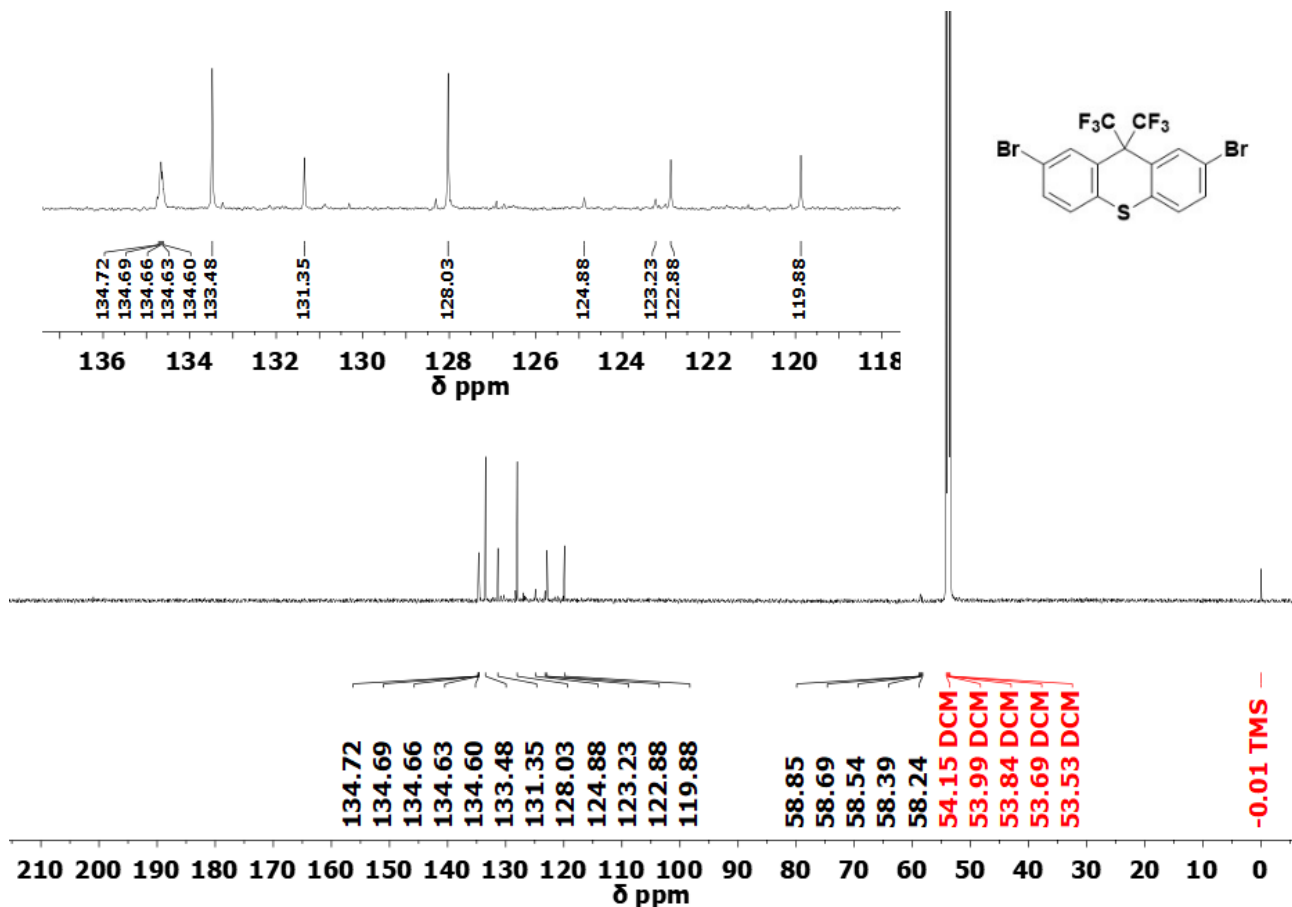
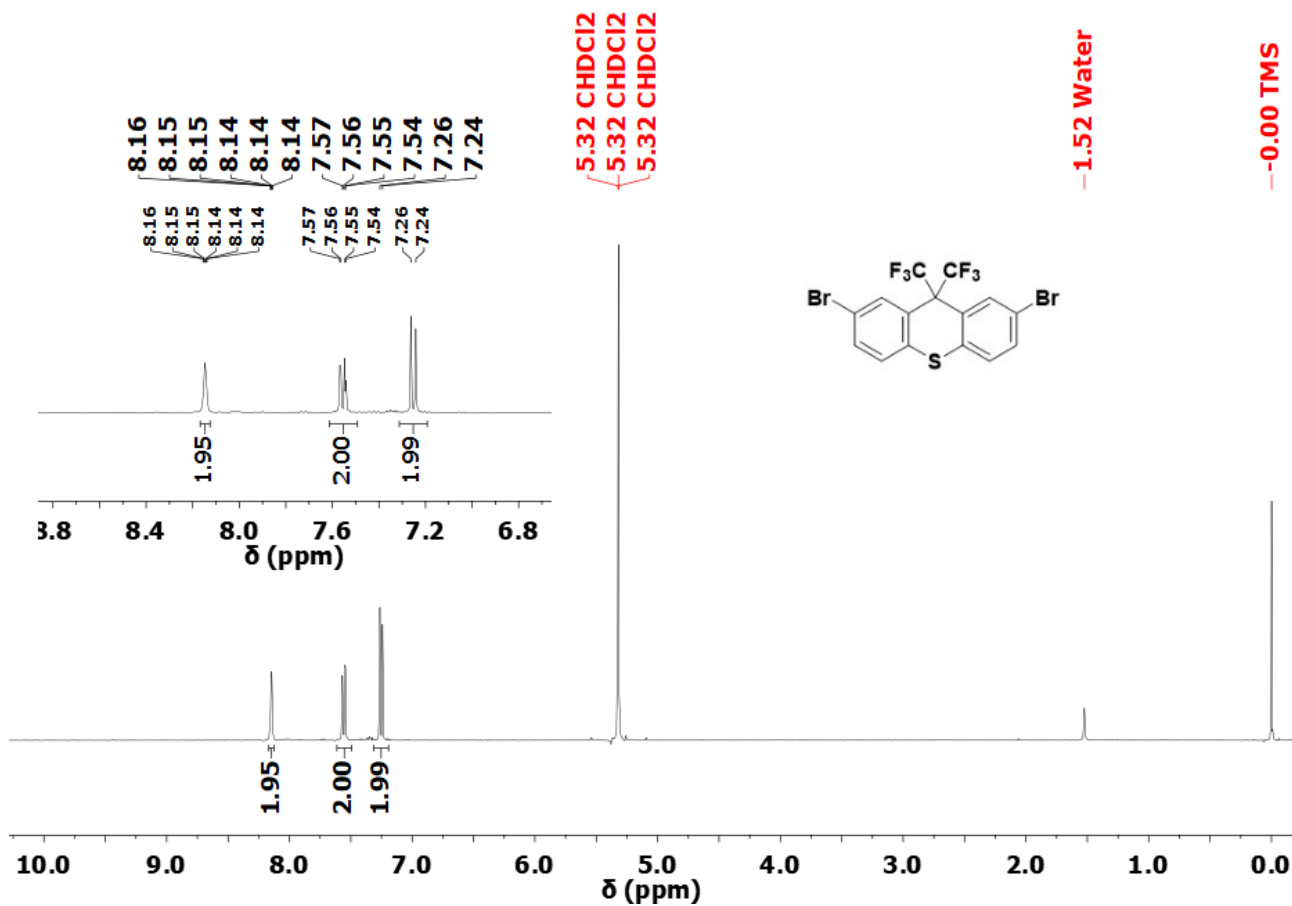
Using general procedure **A**, 2,7-dibromo-9,9-dimethylthioxanthene S,S-dioxide (**19**) (72 mg, 0.172 mmol, 1 eq.), 9,9-dimethyl-2,7-bis(trifluoromethyl)-9,10-dihydroacridine (125 mg, 0.362 mmol, 2.1 eq), toluene (6 mL), Pd₂(dba)₃·CHCl₃ (9 mg, 8.7 μmol, 0.05 eq.), HP^tBu₃BF₄ (5 mg, 17 μmol, 0.10 eq.) and NaO^tBu (50 mg, 0.52 mmol, 3 eq.) were used to make the title compound with 17 h reaction time. Work up was performed as in general procedure **A**. Silica gel column chromatography was performed eluting with gradient DCM: hexane (6:4), increasing to 7:3 (v/v). Removal of solvent under reduced pressure following with trituration with ether gave a thick oil which was with sonicated in pentane (5 mL) to give a white solid which was filtered in a sinter. The product was washed with cold pentane (2 × 5 mL) and was dried under high vacuum overnight to give product as a white solid (92 mg, 56%).

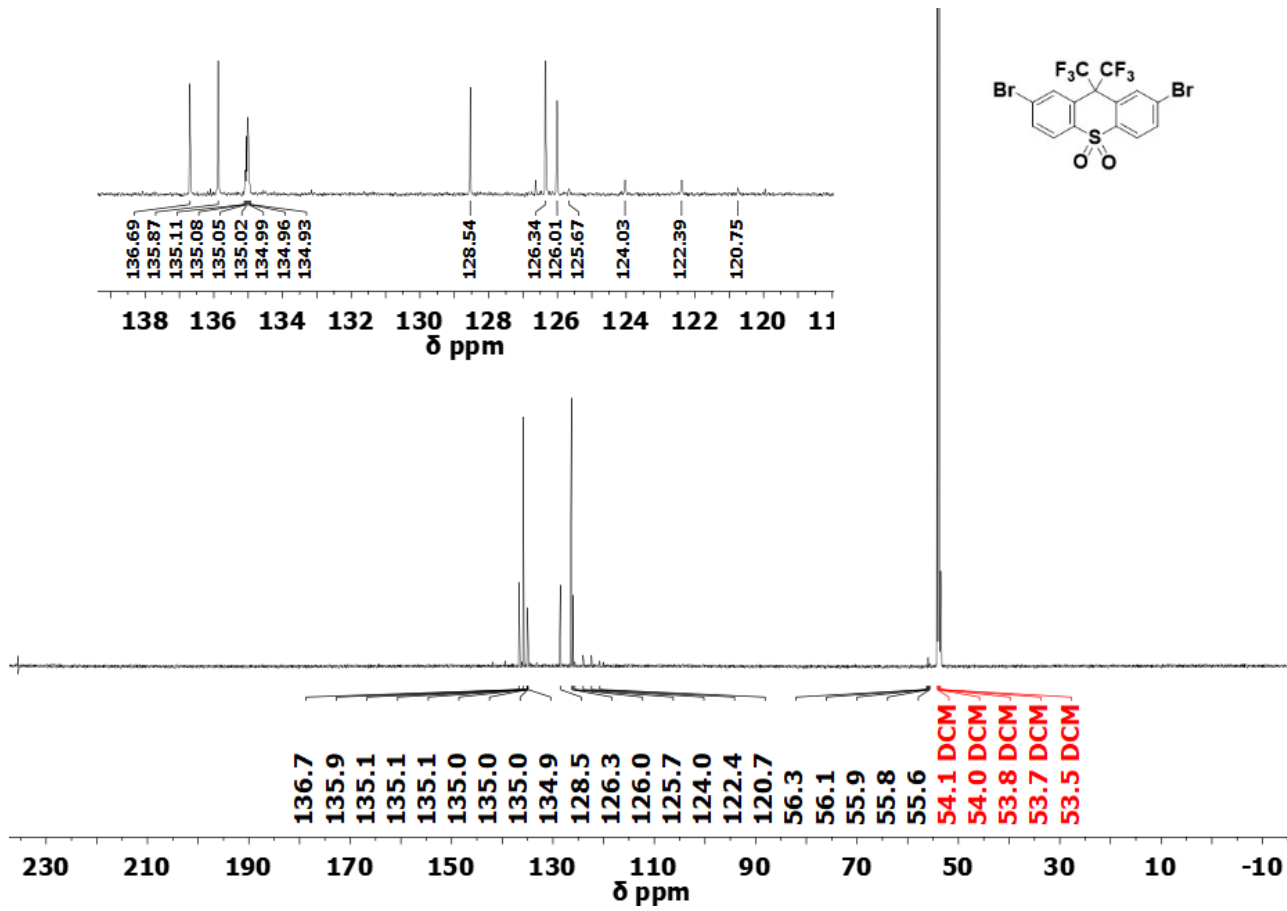
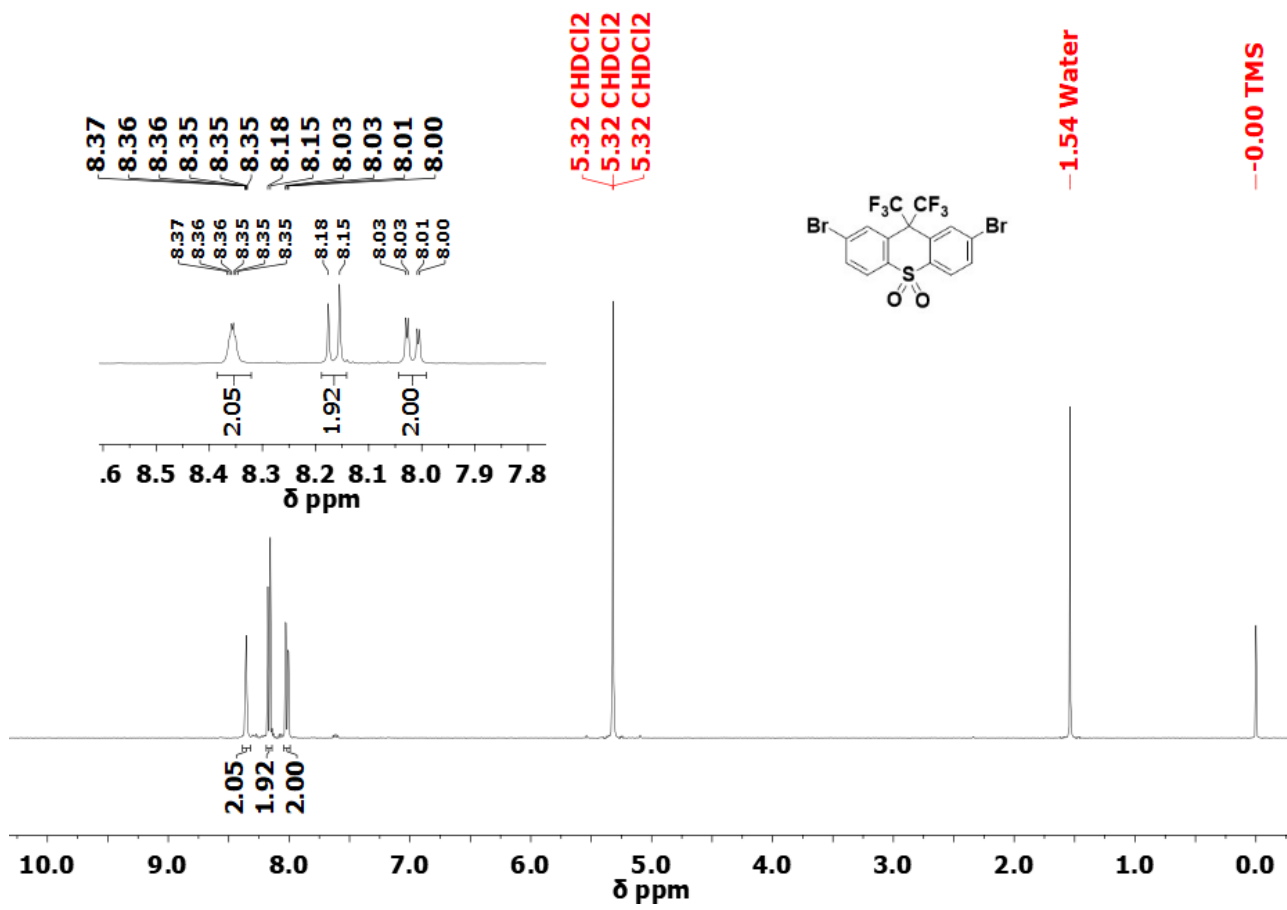
¹H NMR (700 MHz, CD₂Cl₂) δ 8.57 (d, *J* = 8.2 Hz, 2H), 7.75 (apr. t, *J* = 1.8 Hz, 6H), 7.61 (dd, *J* = 8.2, 1.8 Hz, 2H), 7.28 (dd, *J* = 8.7, 1.2 Hz, 4H), 6.35 (d, *J* = 8.7 Hz, 4H), 1.92 (s, 6H), 1.75 (s, 12H); ¹³C NMR (176 MHz, CD₂Cl₂) δ 150.0, 144.8, 142.6, 137.8, 131.0, 130.7, 129.1, 128.2, 125.0 (q, *J* = 272 Hz), 124.4 (q, *J* = 4 Hz), 124.1 (q, *J* = 32 Hz), 123.4 (q, *J* = 4 Hz), 114.8, 40.5, 36.7, 31.8, 31.0; ¹⁹F NMR (376 MHz, CD₂Cl₂) δ -61.9; HRMS-ASAP-TOF⁺ m/z calculated for C₄₉H₃₇F₁₂N₂O₂S [MH]⁺ 945.2379, found: 945.2374. m. p.: 302–304 °C.

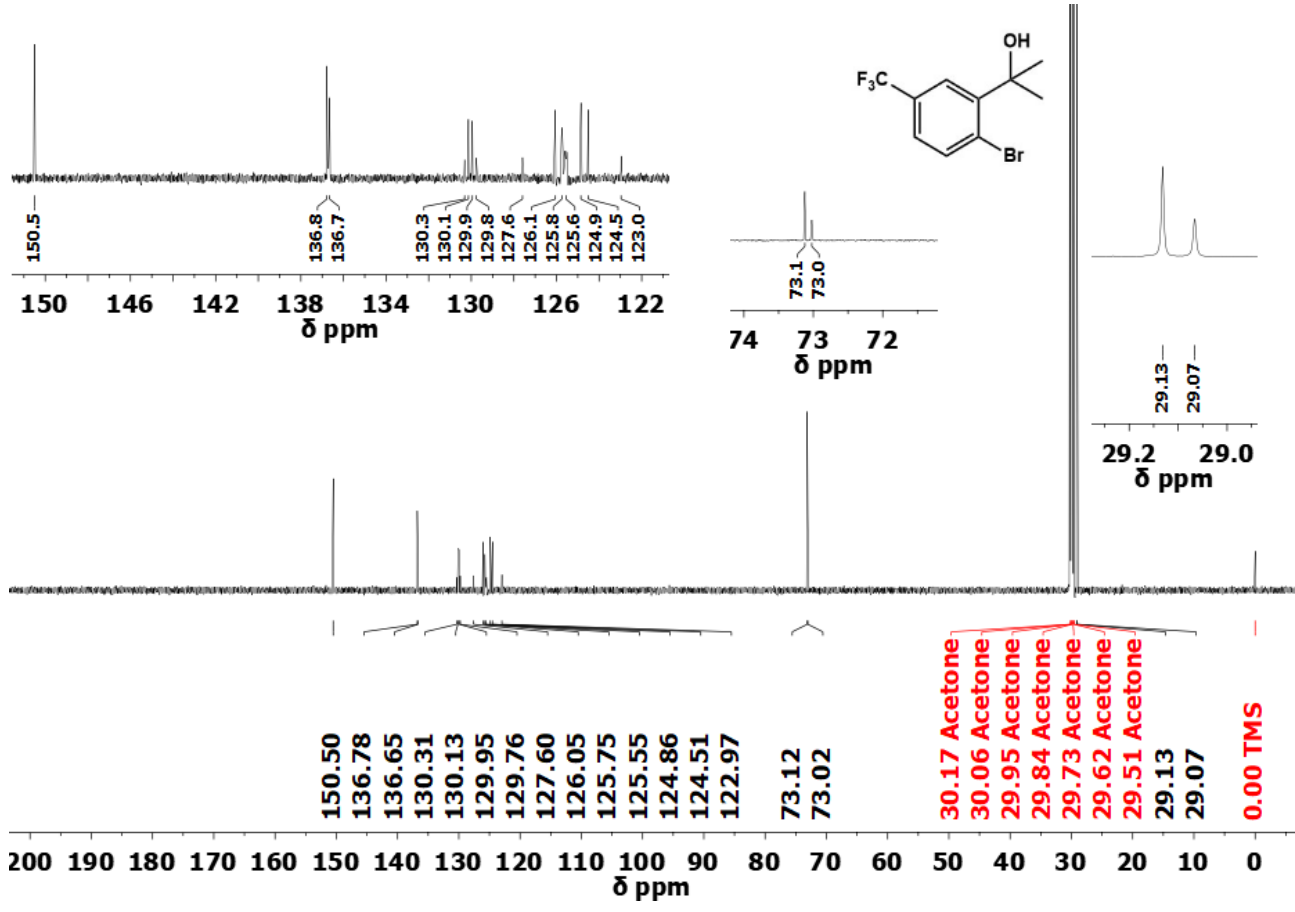
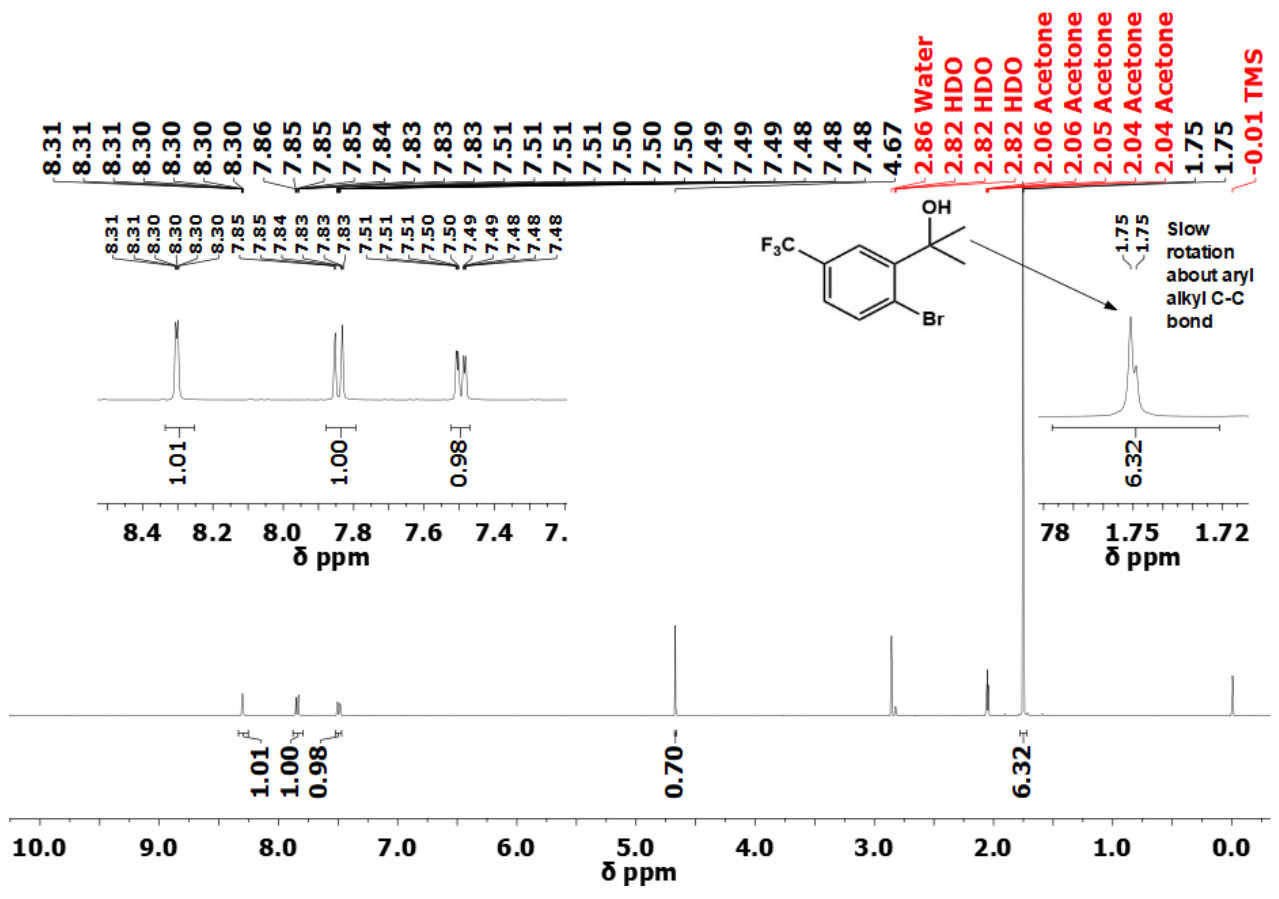
S3 ^1H and $^{13}\text{C}\{^1\text{H}\}$ NMR spectra

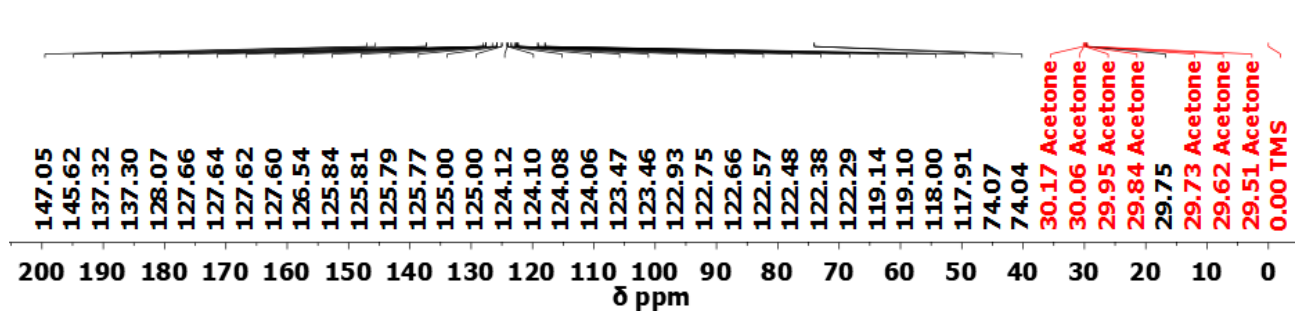
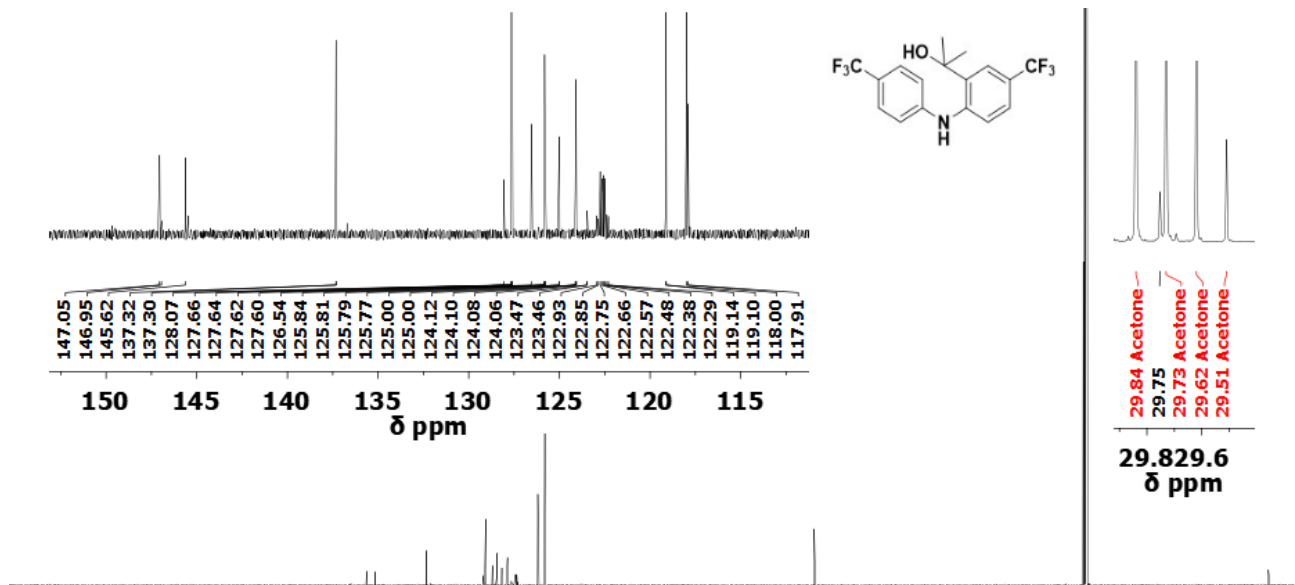
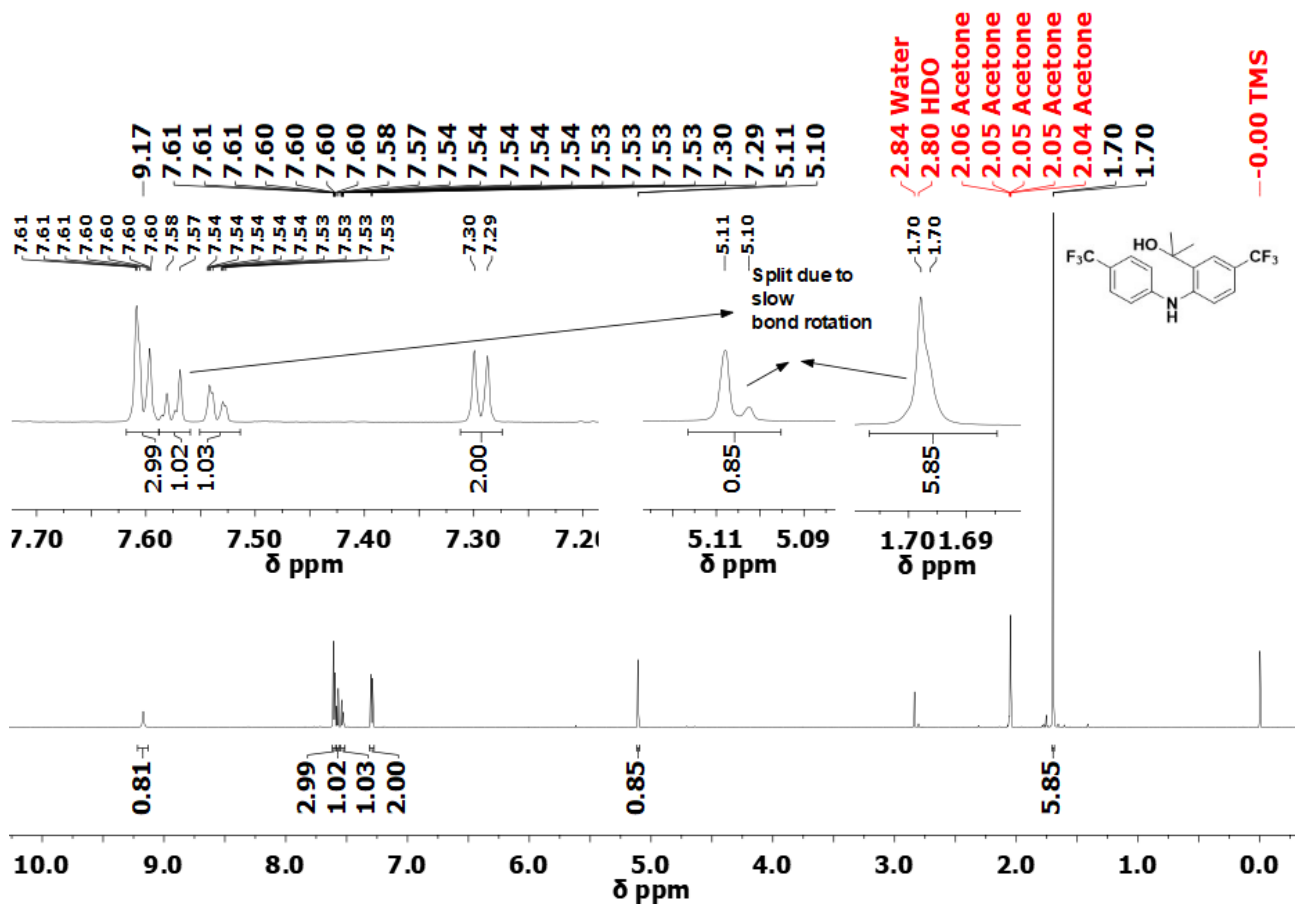


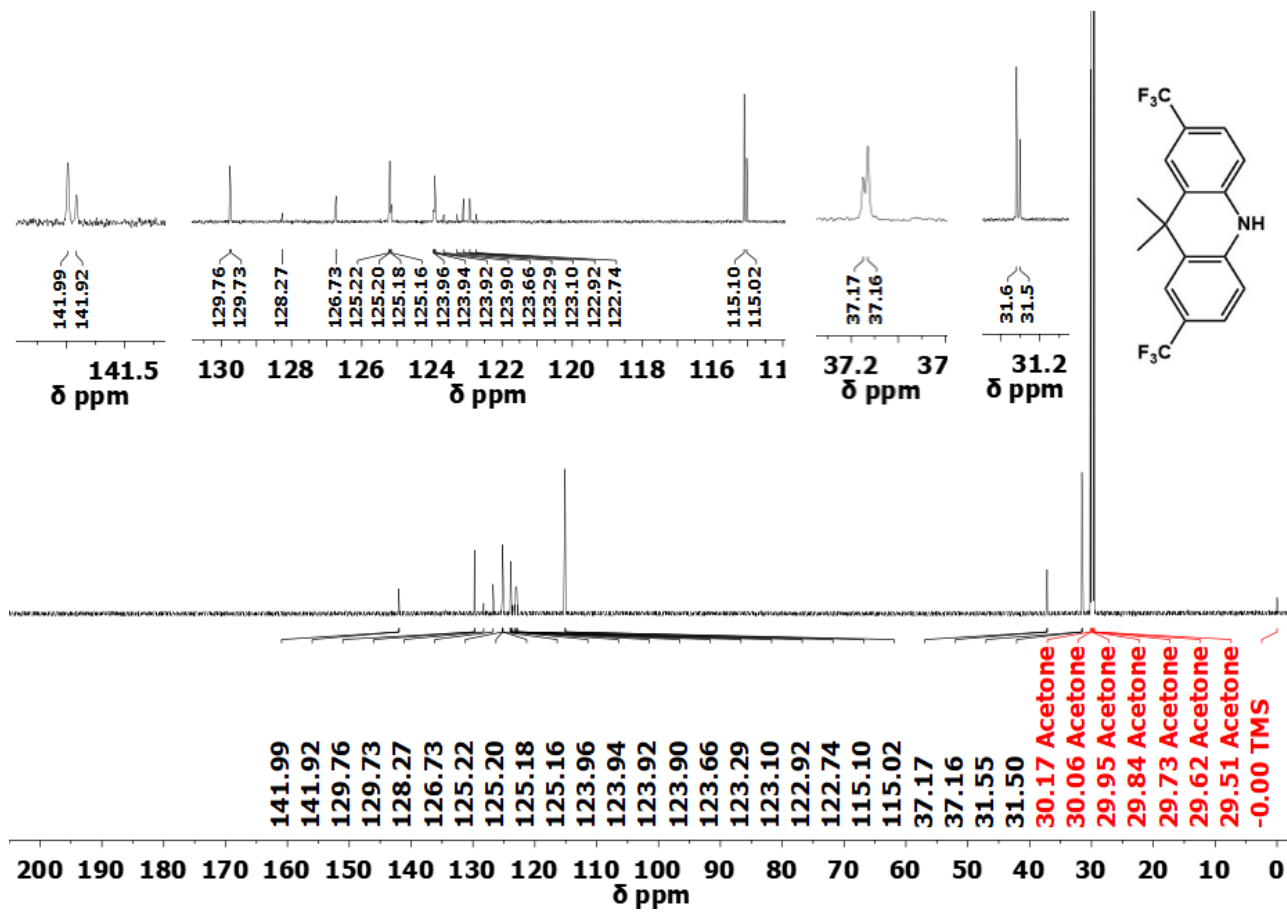
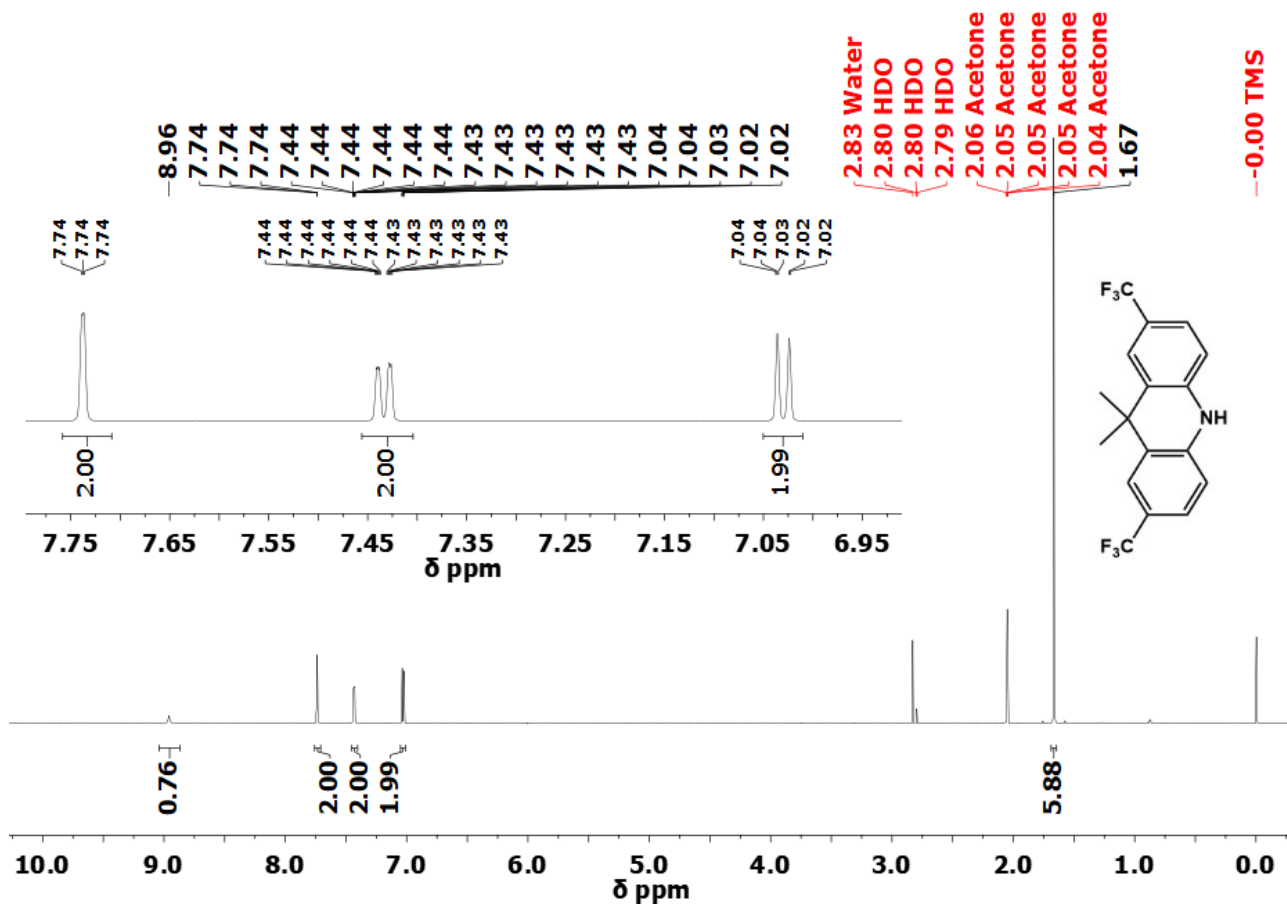


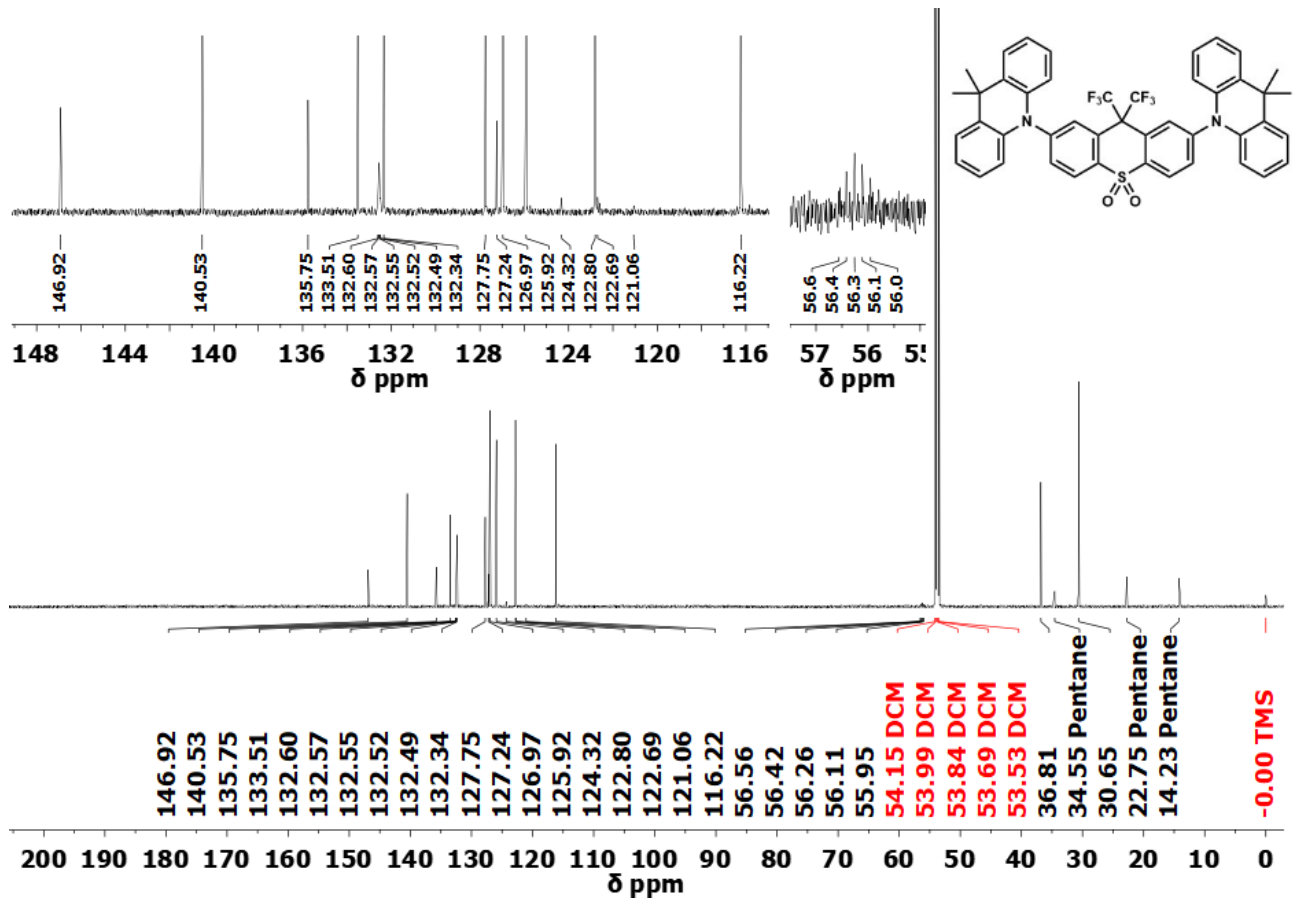
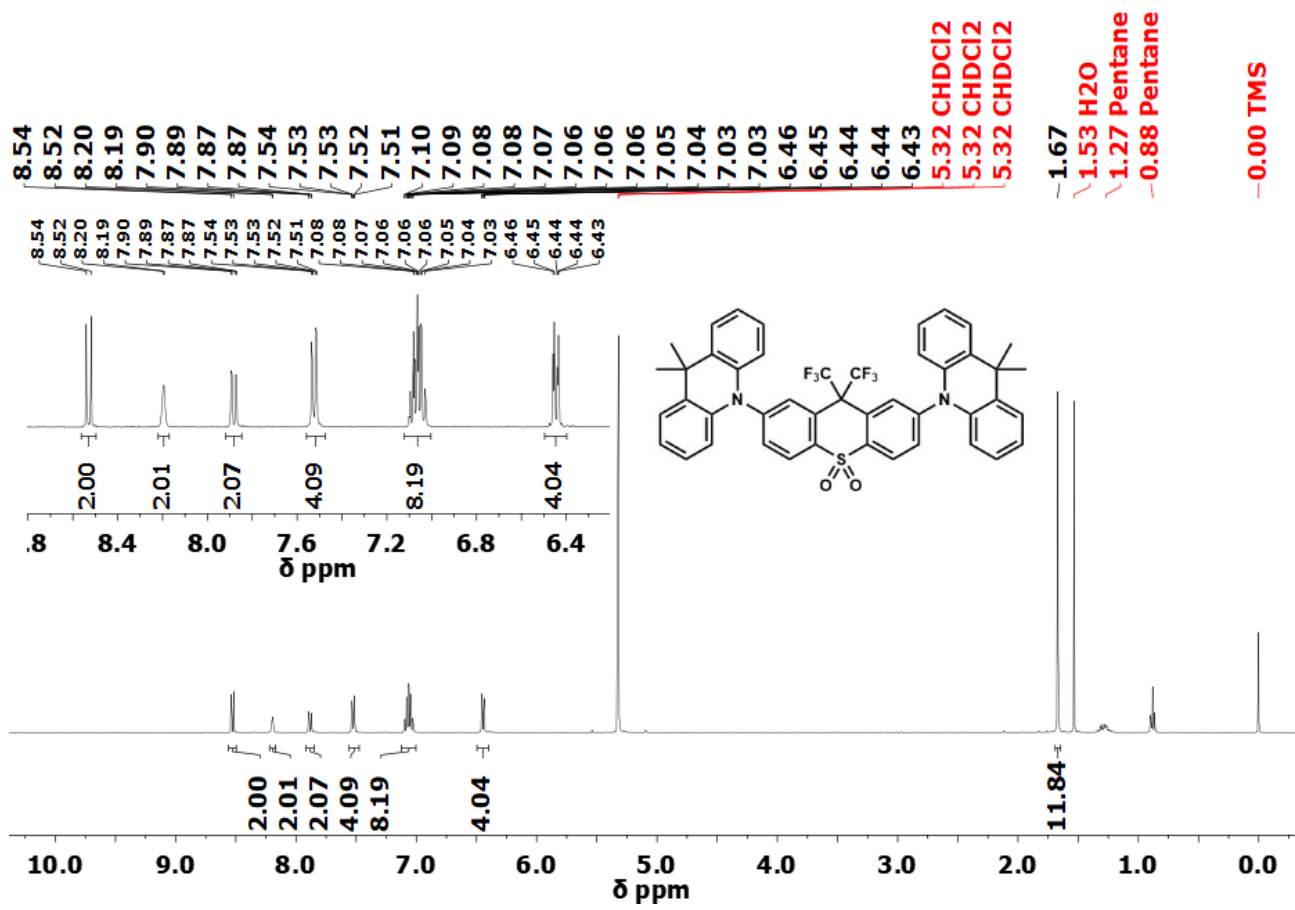


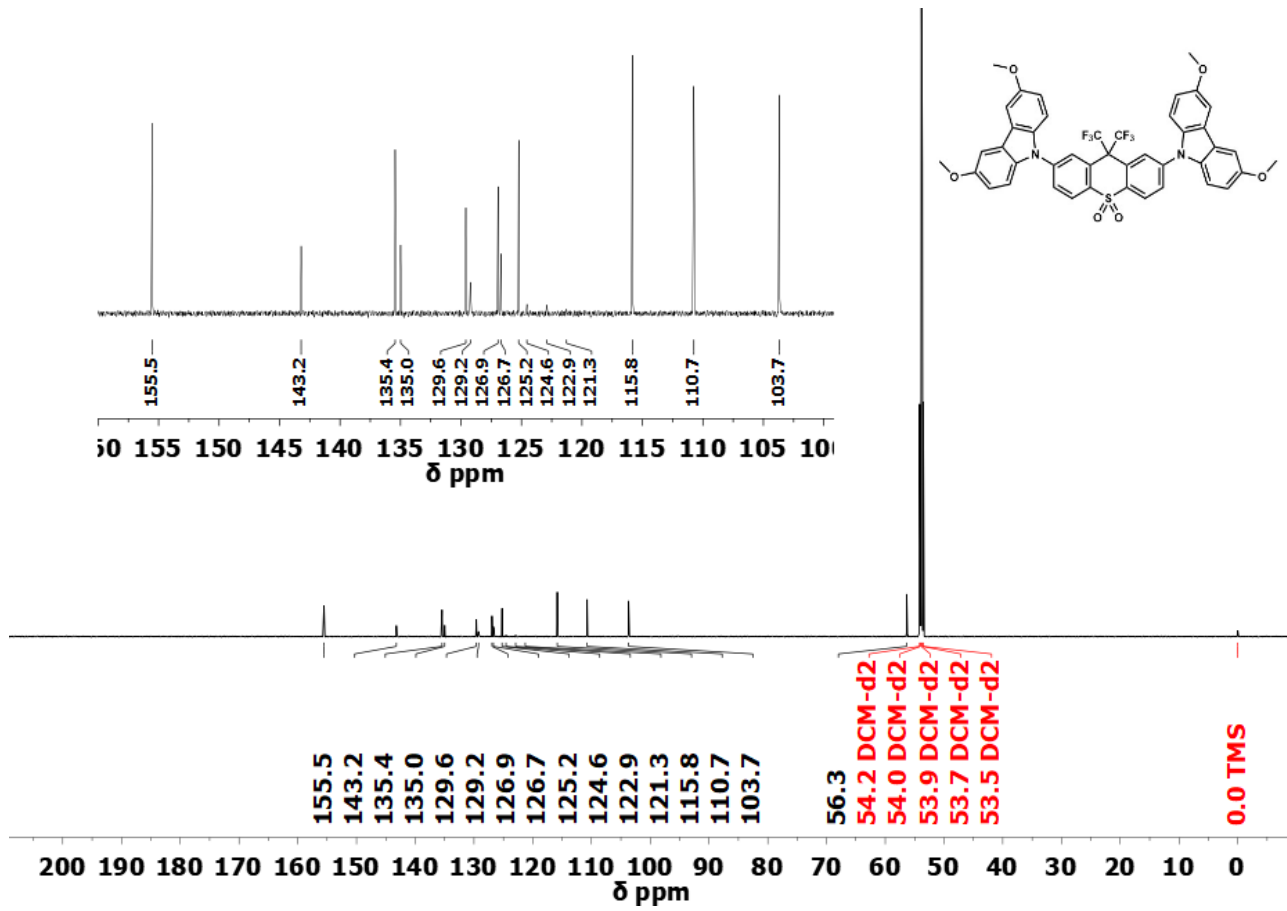
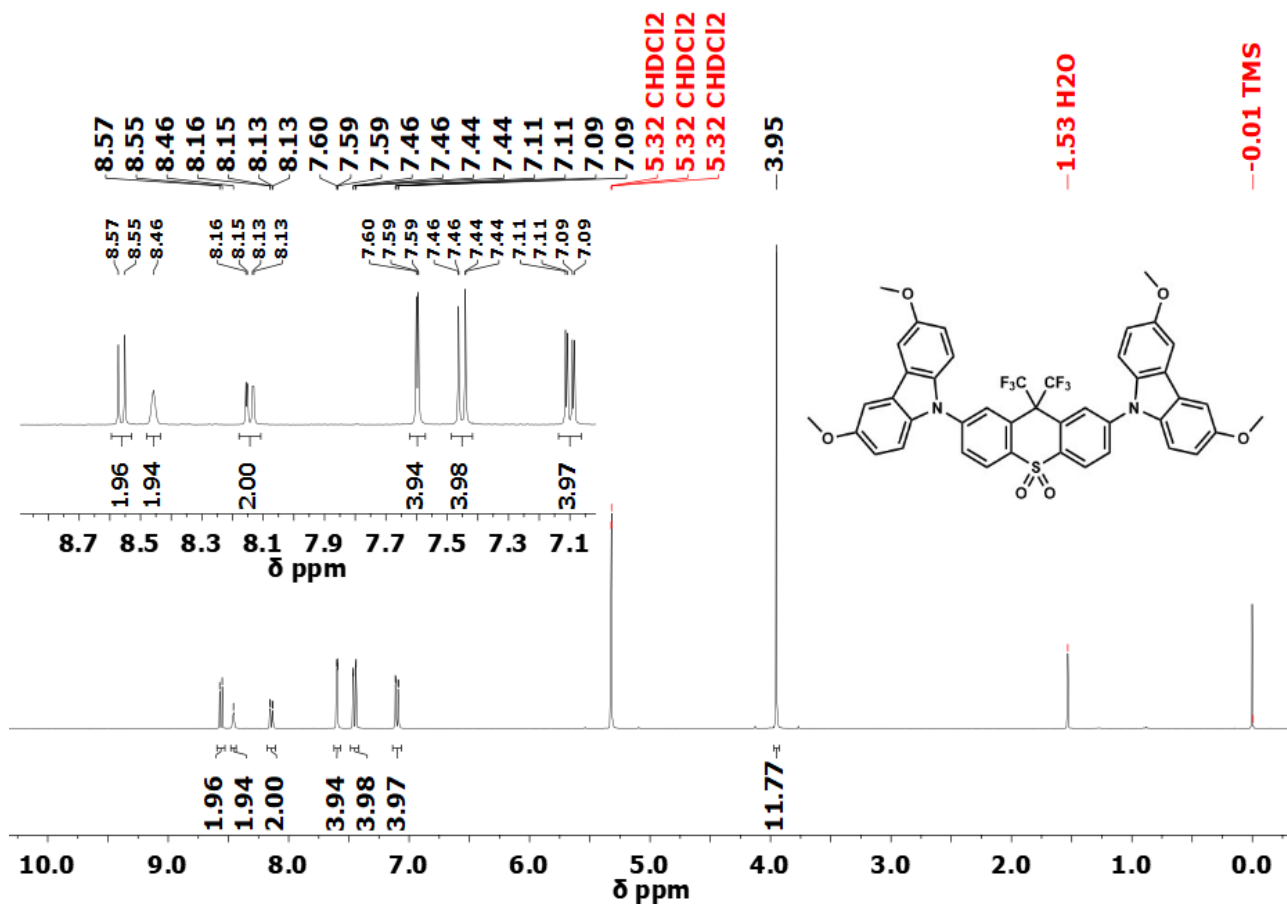


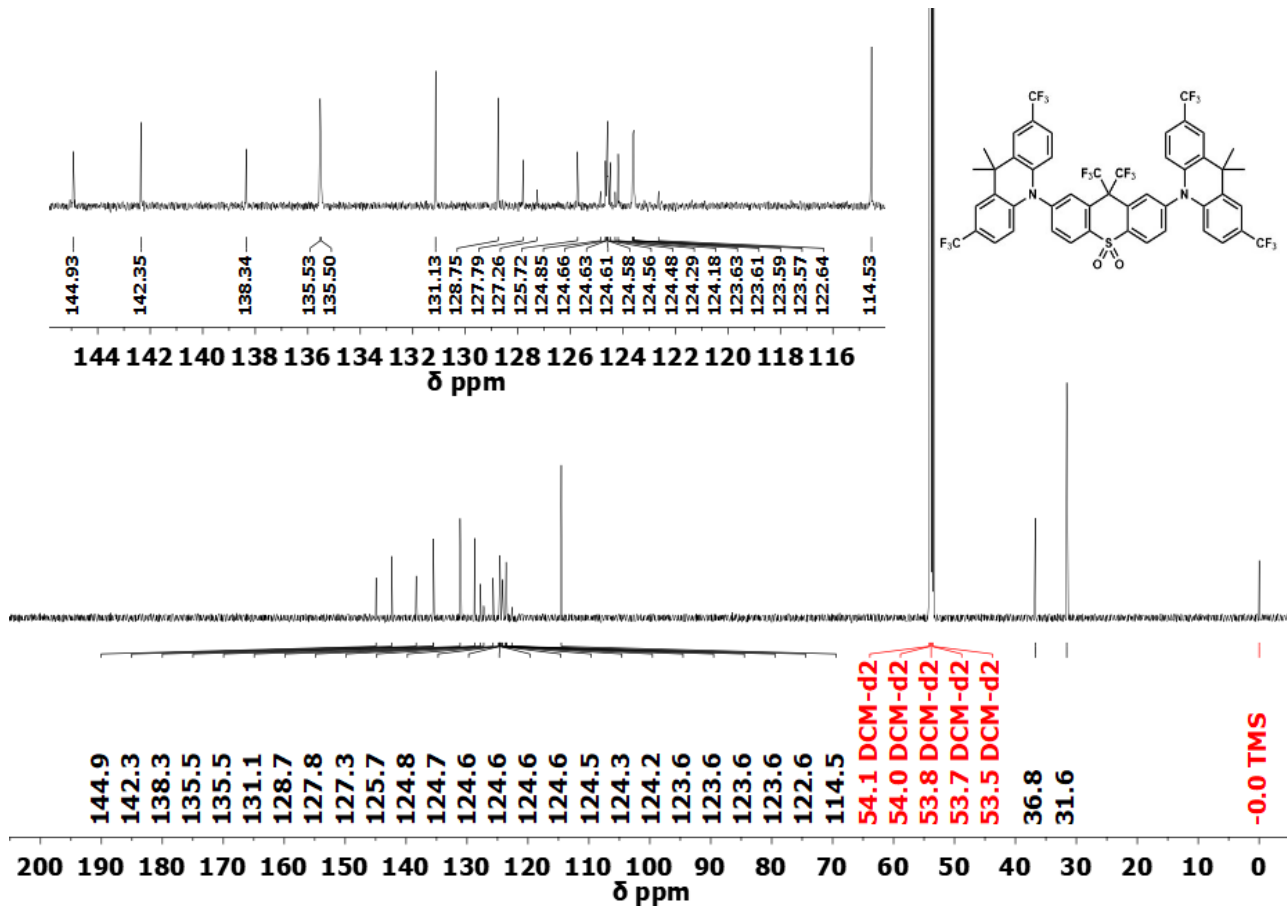
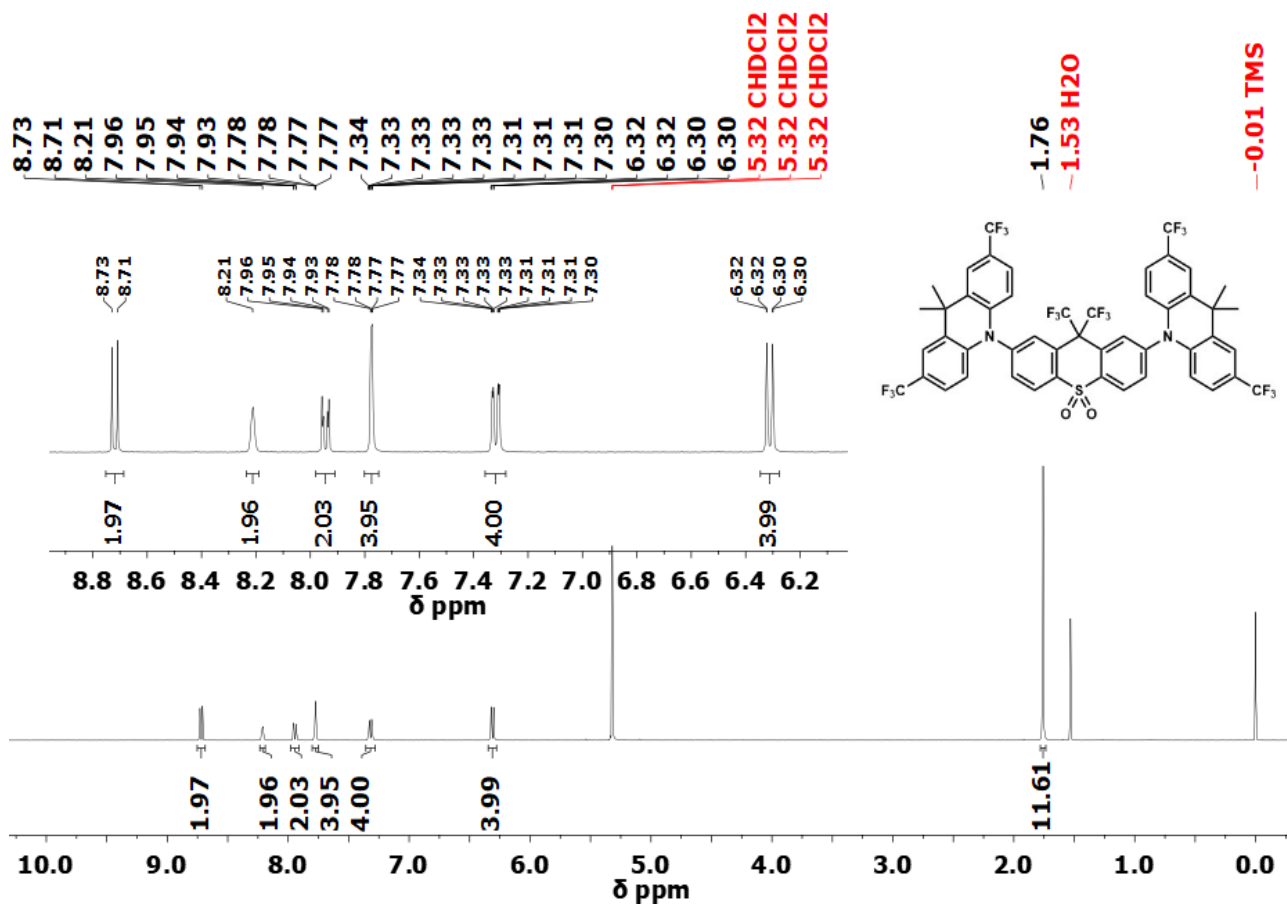


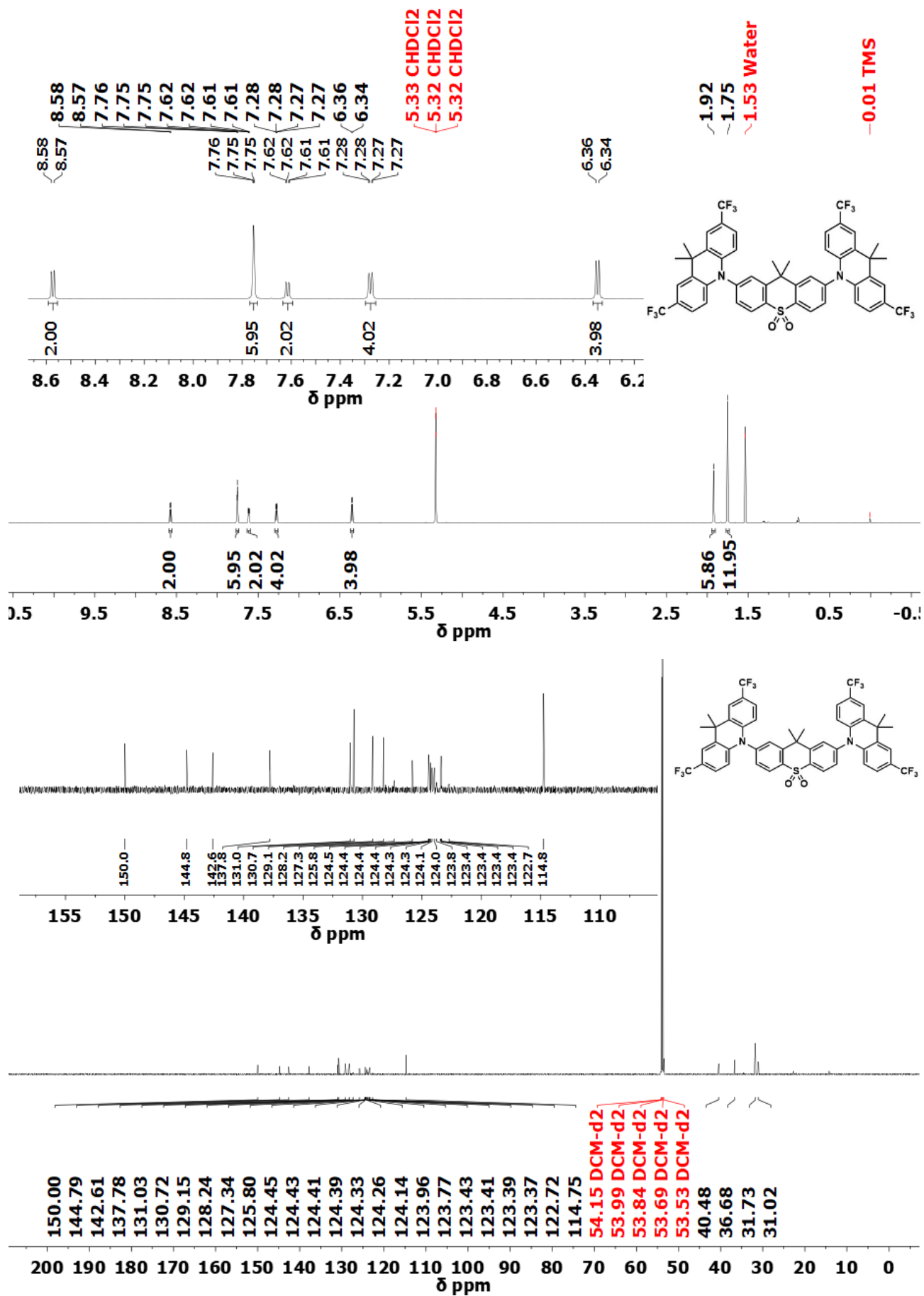












S4 Solution Electrochemical Analysis

Cyclic voltammetry (CV) measurements were performed using a BAS CV50W electrochemical analyzer fitted with a three-electrode system consisting of a glassy carbon ($\phi = 3$ mm) working electrode, and Pt wire counter and quasi reference electrodes. Experiments were conducted at a scan rate of 100 mV s^{-1} . All experiments were conducted in dry deoxygenated MeCN with 0.1 M tetrabutylammonium hexafluorophosphate as the supporting electrolyte. All voltammograms presented in **Figure 3** were referenced using separate voltammograms with internal ferrocene (**Figure S4a**). The HOMO and LUMO levels in **Table 1** were obtained from the onsets of the redox waves using the equations $\text{HOMO} \sim \text{ionization potential (IP)} = |e|(E_{\text{ox}(\text{onset})} + 5.1) \text{ eV}$ and $\text{LUMO} \sim \text{electron affinity (EA)} = -|e|(E_{\text{red}(\text{onset})} + 5.1) \text{ eV}$. The $+5.1 \text{ V}$ value is the ferrocene/ferrocenium couple potential.

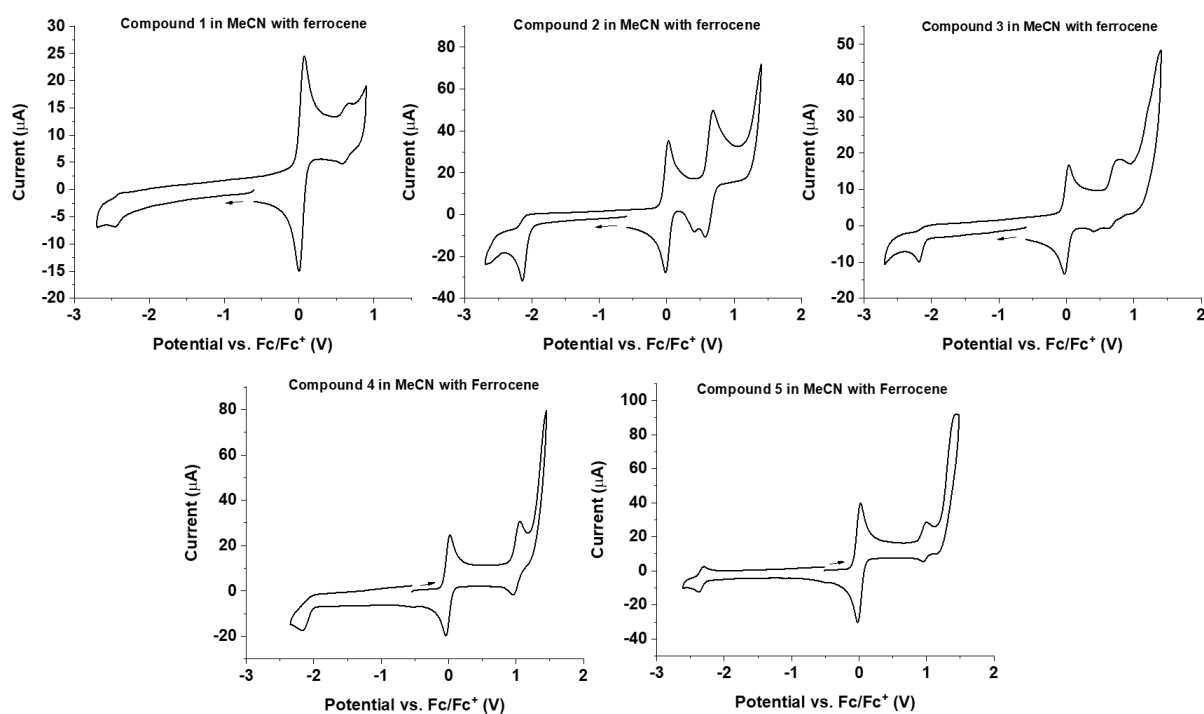


Figure S4a CV for compounds **1–5** in deoxygenated MeCN with internal ferrocene referenced to 0 V. Arrows indicate the initial scan direction for each compound.

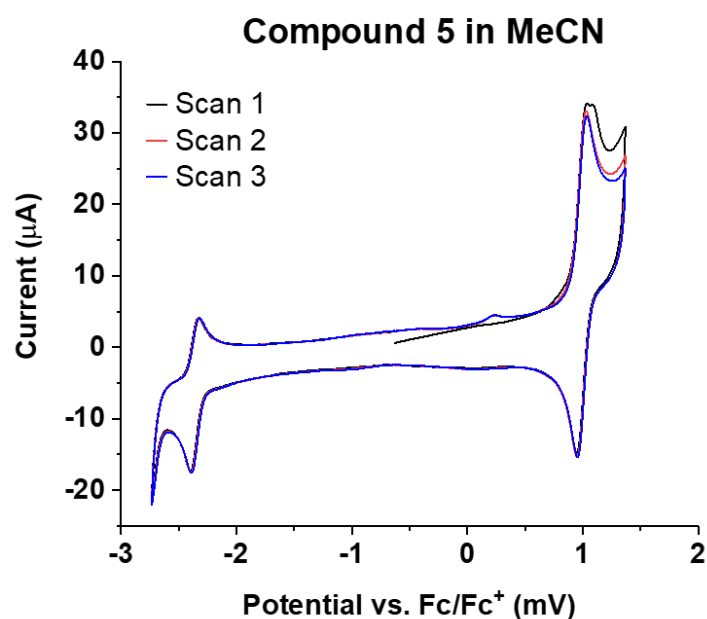


Figure S4b CV for compound **5** in MeCN with three continuous oxidation and reduction cycles showing the high degree of reversibility for both the oxidation and reduction.

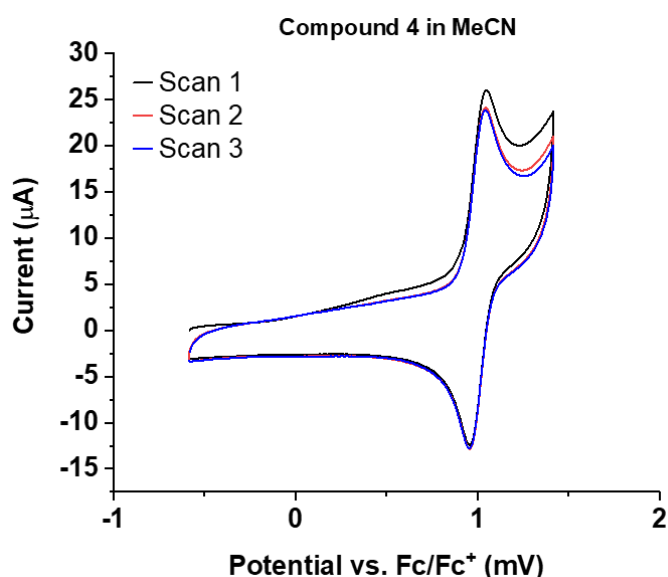


Figure S4c CV for compound **4** with three continuous oxidation cycles showing the high degree of reversibility for the oxidation.

S5 Photophysical and optoelectronic data

General photophysical experimental details

Three types of samples were studied in this work. Solutions in organic solvents (10^{-3} to 10^{-5} M) were diluted from 1 mg mL^{-1} stock solutions. Drop-cast films were produced by deposition onto quartz or sapphire substrates preheated to $70 \text{ }^\circ\text{C}$ on a hotplate, from toluene solutions containing the emitter and polymeric host Zeonex (1 wt.% emitter) or other small molecule host (10 wt.% emitter). For

PLQY measurements of material **4**, additional thin film samples (100 nm thickness, 25 vol.% emitter) were thermally evaporated onto sapphire substrates using a Kurt J. Lesker Super Spectros 200 deposition ($\approx 10^{-7}$ Torr chamber pressure and 1 \AA s^{-1} deposition rates) in DPEPO by QCM-monitored rate-controlled codeposition.

Steady-state absorption and emission spectra were acquired using a UV-3600 Shimadzu spectrophotometer and a JobinYvon Horiba Fluoromax 3, respectively. Time-resolved spectra were obtained by exciting the sample with a Nd:YAG laser (EKSPLA, 10 Hz, 355 nm) Sample emission was directed onto a spectrograph and gated iCCD camera (Stanford Computer Optics). For previous development of these methods see the literature.¹⁰ PLQYs were measured using a calibrated Quanta- ϕ integrating sphere with coupled Jobin Yvon FluoroLog-3 spectrometer with PMT detector (0.5 s integration time) and analyzed using FluorEssence software. The sphere was flushed with N₂ for 30 min prior to measurement to prevent triplet quenching by atmospheric oxygen, and the excitation wavelength for PLQYs was 330 nm with 5 nm bandpass.

OLED devices (pixel size alternatively 2×2 mm, 2×4 mm or 4×4 mm) were fabricated on patterned ITO coated glass (VisionTek Systems) with a sheet resistance of $15 \text{ } \Omega/\text{sq}$. The substrates were sonicated for 15 min each in acetone and then *isopropyl* alcohol (IPA). After further oxygen-plasma cleaning, the substrates were loaded into a Kurt J. Lesker Super Spectros 200 deposition chamber. All organic and cathode layers were thermally evaporated at a pressure below 10^{-7} mbar, at evaporation rates in the range of $0.1\text{--}0.5 \text{ \AA/s}$. The materials used for the device fabrication were: *N,N'*-bis-(naphthalene-1-yl)-*N,N'*-bis(phenyl)benzidine (NPB) (Lumtec), 4,4-(diphenylsilanediy)bis(*N,N*-diphenylaniline) (TSBPA) (Lumtec), 1,3,5-tris(*N*-phenylbenzimidazol-2-yl)benzene (TPBi) (Lumtec), bis[2-(diphenylphosphino)phenyl]ether oxide (DPEPO) (Sigma Aldrich), UGH3 (Sigma), BCPO (Lumtec), 2CzCbPy (gift provided by Merck, see literature for information),¹¹ mCP (Sigma), lithium fluoride (LiF), (99.995%, Sigma Aldrich), and aluminium (99.9995%, Alfa Aesar). With the exception of compound **2**, all compounds were either purchased presublimed or were sublimed before use in a Creaphys sublimation system. Characterization of the OLED devices was conducted in a 10-inch calibrated integrating sphere (Labsphere) coupled with a calibrated fibre spectrometer (Ocean Optics USB4000) and connected to a Keithley 2400 source measure unit.

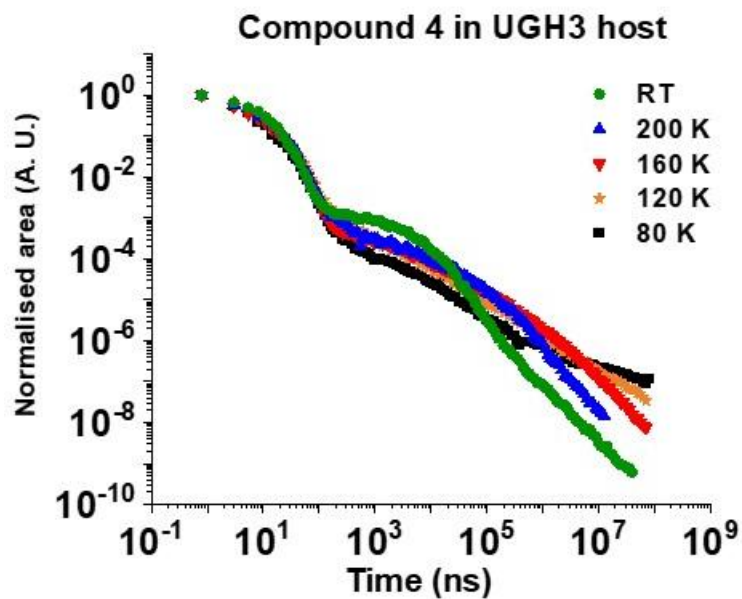


Figure S5a. Time resolved photoluminescence decays at varying temperatures for drop cast films of compound 4 at 10 wt.% in UGH3 host matrix. The data shows the temperature dependence of the delayed fluorescence in the late ns and early μ s region of the decay.

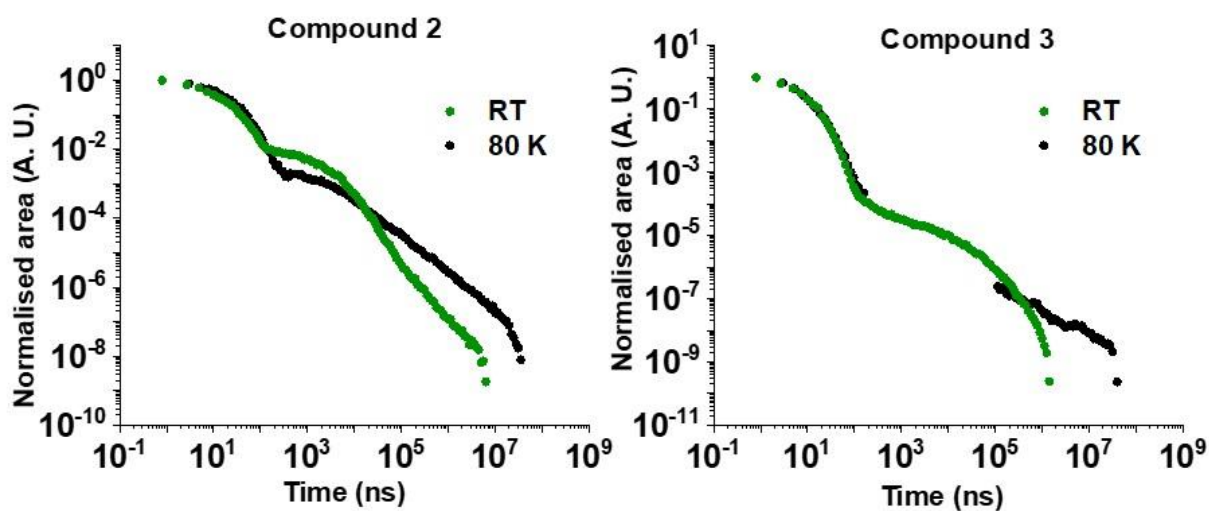


Figure S5b Time resolved photoluminescence decays at varying temperatures for drop cast films of compounds 2 and 3 at 10 wt.% in DPEPO host matrix. The data shows the temperature dependence of the delayed fluorescence in the late ns and early μ s region of the decay.

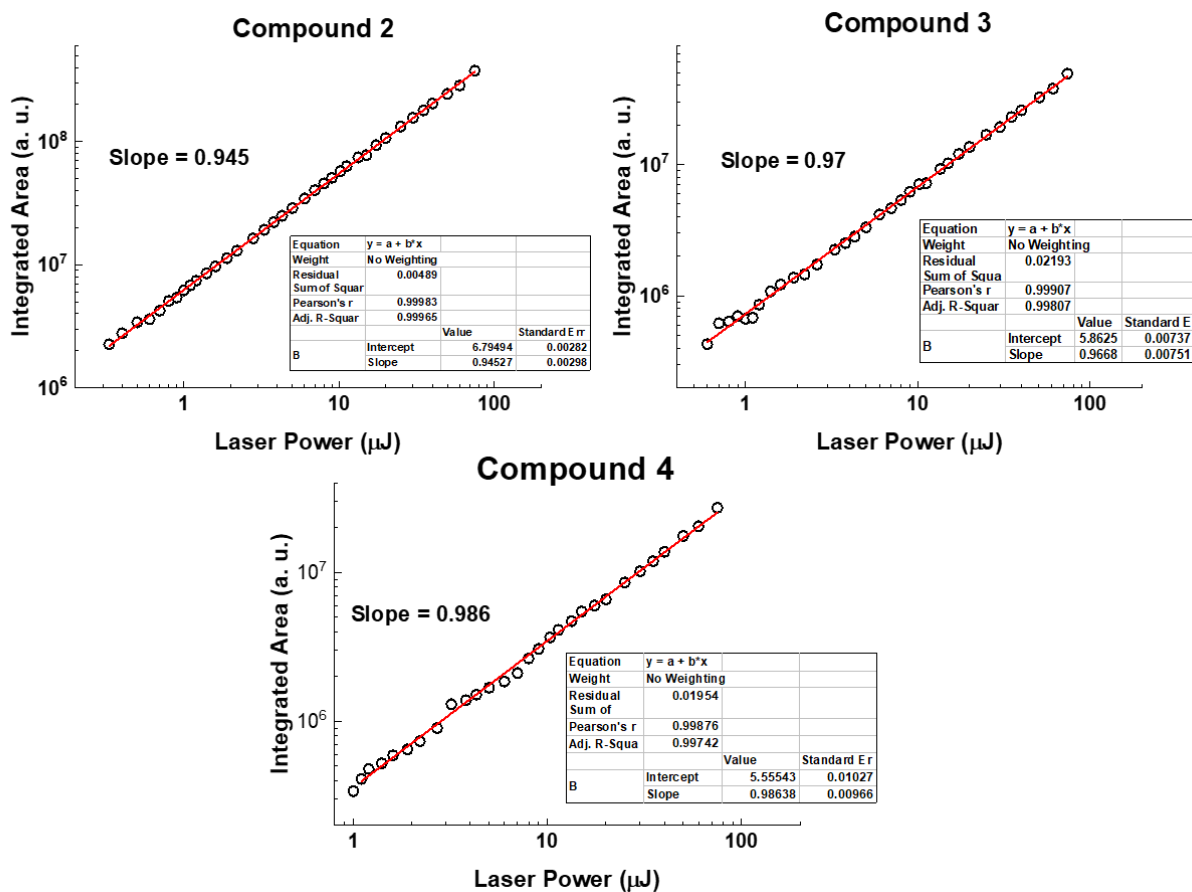


Figure S5c Power dependence experiments for compounds **2–4** in DPEPO host. In all cases emission was collected exclusively from the delayed emission (CCD integration from 300-900 ns after laser excitation for material **2**, 1-4.5 μ s for material **3**, and 500-700 ns for material **4**).

Table S1 Fitting parameters for emission lifetimes of 1-5 at 10 wt.% in drop cast DPEPO films

Compound 1							
Model	ExpDecay2	PF		Model	ExpDecay2	DF	
Equation	$y = y_0 + A_1 \cdot \exp(-(x-x_0)/\tau_1) + A_2 \cdot \exp(-(x-x_0)/\tau_2)$			Equation	$y = y_0 + B_1 \cdot \exp(-(x-x_0)/\tau_1) + B_2 \cdot \exp(-(x-x_0)/\tau_2)$		
Adj. R-Square	0.9975			Adj. R-Square	0.9959		
		Value	Standard Error			Value	Standard Error
CALC	y0	0	0	CALC	y0	0	0
CALC	x0	0.8	0	CALC	x0	429.7	0
CALC	A ₁	9.08E+07	5871524.448	CALC	B ₁	1237161	44439.19556
CALC	τ ₁ (ns)	6.49638	0.62963	CALC	τ ₁ (ns)	2471.454	146.52136
CALC	A ₂	5.59E+07	6001231.953	CALC	B ₂	2932836	46052.54926
CALC	τ ₂ (ns)	28.8222	1.86835	CALC	τ ₂ (ns)	11603.74	1080.36154
Compound 2							
Model	ExpDecay2	PF		Model	ExpDecay2	DF	
Equation	$y = y_0 + A_1 \cdot \exp(-(x-x_0)/\tau_1) + A_2 \cdot \exp(-(x-x_0)/\tau_2)$			Equation	$y = y_0 + B_1 \cdot \exp(-(x-x_0)/\tau_1) + B_2 \cdot \exp(-(x-x_0)/\tau_2)$		
Adj. R-Square	0.9989			Adj. R-Square	0.9957		
		Value	Standard Error			Value	Standard Error
CALC	y0	0	0	CALC	y0	0	0
CALC	x0	0.8	0	CALC	x0	184.5	0
CALC	A ₁	1.09E+07	581250.4051	CALC	B ₁	1188179	5396.419
CALC	τ ₁ (ns)	3.97984	0.30407	CALC	τ ₁ (ns)	1075.874	85.97147
CALC	A ₂	9971562.586	588751.6547	CALC	B ₂	60621.22	5532.59414
CALC	τ ₂ (ns)	24.45933	1.34111	CALC	τ ₂ (ns)	6028.903	376.54099
Compound 3							
Model	ExpDecay2	PF		Model	ExpDecay2	DF	
Equation	$y = y_0 + A_1 \cdot \exp(-(x-x_0)/\tau_1) + A_2 \cdot \exp(-(x-x_0)/\tau_2)$			Equation	$y = y_0 + B_1 \cdot \exp(-(x-x_0)/\tau_1) + B_2 \cdot \exp(-(x-x_0)/\tau_2)$		
Adj. R-Square	0.9978			Adj. R-Square	0.9845		
		Value	Standard Error			Value	Standard Error
CALC	y0	0	0	CALC	y0	0	0
CALC	x0	0.8	0	CALC	x0	339.7	0
CALC	A ₁	1.36E+08	1.27E+07	CALC	B ₁	4462.302	209.80318
CALC	τ ₁ (ns)	3.51144	0.37577	CALC	τ ₁ (ns)	15650.74	1010.64587
CALC	A ₂	8.69E+07	1.30E+07	CALC	-	-	-
CALC	τ ₂ (ns)	10.88483	0.66167	CALC	-	-	-
Compound 4							
Model	ExpDecay2	PF		Model	ExpDecay2	DF	
Equation	$y = y_0 + A_1 \cdot \exp(-(x-x_0)/\tau_1) + A_2 \cdot \exp(-(x-x_0)/\tau_2)$			Equation	$y = y_0 + B_1 \cdot \exp(-(x-x_0)/\tau_1) + B_2 \cdot \exp(-(x-x_0)/\tau_2)$		
Adj. R-Square	0.9994			Adj. R-Square	0.9911		
		Value	Standard Error			Value	Standard Error
CALC	y0	0	0	CALC	y0	0	0
CALC	x0	0.8	0	CALC	x0	544.6511	0
CALC	A ₁	3.18E+07	2.44E+06	CALC	B ₁	51238.03	2157.03936
CALC	τ ₁ (ns)	2.39085	0.21983	CALC	τ ₁ (ns)	2154.611	178.6593
CALC	A ₂	3.81E+07	2.45E+06	CALC	B ₂	21050.96	1984.50814
CALC	τ ₂ (ns)	11.77197	0.5892	CALC	τ ₂ (ns)	17794.28	1470.20612
Compound 5							
Model	ExpDecay2	PF					
Equation	$y = y_0 + A_1 \cdot \exp(-(x-x_0)/\tau_1) + A_2 \cdot \exp(-(x-x_0)/\tau_2)$						
Adj. R-Square	0.9969						
		Value	Standard Error				
CALC	y0	0	0				
CALC	x0	0.8	0				
CALC	A ₁	7.52E+04	8.62E+04				
CALC	τ ₁ (ns)	12.94447	10.22692				
CALC	A ₂	-	-				
CALC	τ ₂ (ns)	-	-				

Table S2 The following OLED stacks were investigated, representing variations upon the stack of ITO | NPB (40 nm) | TSBPA (10 nm) | EML of 35% emitter in DPEPO (30 nm) | DPEPO (10 nm) | TPBi (40 nm) | LiF/Al previously optimized for material **1**. Additional layers of mCP or removing the DPEPO layer were also investigated to modify charge injection into the EML, although with no discernible change in device performance. Different EML hosts with different charge transport properties (DPEPO electron transporting, mCP hole transporting, 2CzCbPy ambipolar) were also found to have little effect on the timescale of device degradation.

<u>Common layers</u>	EBL	EML	HBL	<u>Common layers</u>
NPB (40nm) TSBPA (10nm)	-	Undoped 4 (7nm)	DPEPO (10nm)	TPBi (40 nm) LiF/Al
	-	Undoped 4 (14nm)	DPEPO (10nm)	
	-	Undoped 4 (25nm)	DPEPO (10nm)	
	-	15% of 4 in DPEPO (30nm)	DPEPO (10nm)	
	-	25% of 4 in DPEPO (30nm)	DPEPO (10nm)	
	-	35% of 4 in DPEPO (30nm)	DPEPO (10nm)	
	mCP (10nm)	15% of 4 in DPEPO (30nm)	-	
	mCP (10nm)	25% of 4 in DPEPO (30nm)	-	
	mCP (10nm)	35% of 4 in DPEPO (30nm)	-	
	mCP (10nm)	15% of 4 in mCP (30nm)	-	
	mCP (10nm)	25% of 4 in mCP (30nm)	-	
	mCP (10nm)	35% of 4 in mCP (30nm)	-	
	mCP (10nm)	15% of 4 in 2CzCbPy (30nm)	-	
	mCP (10nm)	25% of 4 in 2CzCbPy (30nm)	-	
	mCP (10nm)	35% of 4 in 2CzCbPy (30nm)	-	
	-	30% of 2 in BCPO (30nm)	-	
-	30% of 2 in DPEPO (30nm)	-		
-	30% of 2 in 2CzCbPy (30nm)	-		

In all such devices, rapid and irreversible brightness decay was observed at constant voltage driving. Attempts to obtain full V-I-L curves and EL spectra were frustrated by this decay, which occurred on timescales faster than emission collection. Instead, still images from a video of a representative device operating at constant voltage (**Figure S5d**), and a modified V-I-L sweep initiated above the turn-on voltage (thus avoiding some brightness decay at lower voltages, **Figure S5e**) demonstrate the observed instability for these materials.

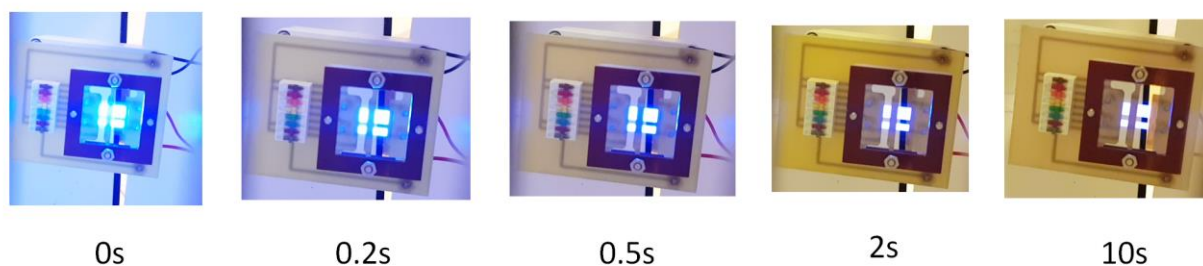


Figure S5d Rapid decay in OLED brightness at constant driving voltage for compound **4** in mCP. This behaviour is representative of all OLEDs using material **2** or **4** as emitter.

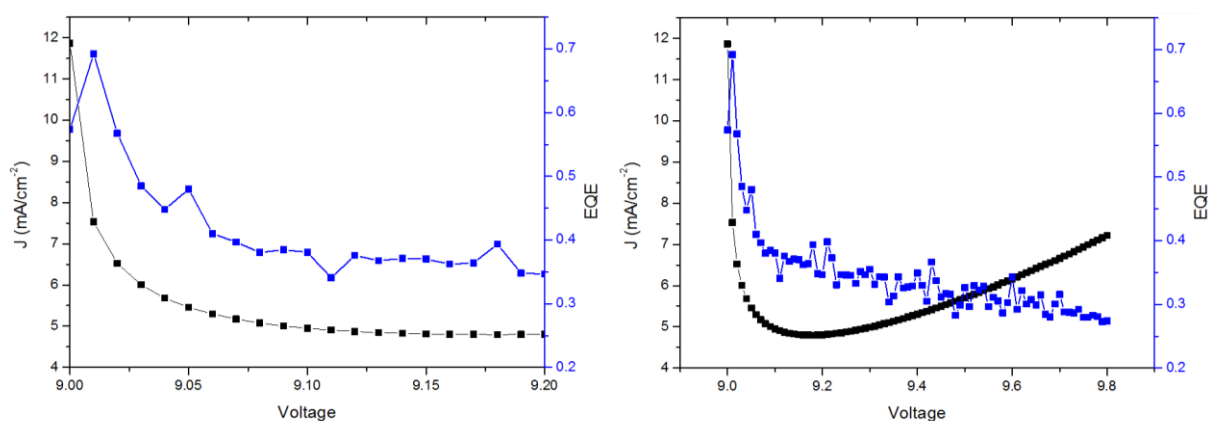


Figure S5e Rapid decay of OLED current (black) and EQE (blue) at quasi-constant driving voltage for compound **4** in mCP (4×4 mm pixel). To avoid electrical stress below the turn-on voltage, on a single pixel the voltage was initially set at 9 V and increased in 0.01 V increments, dwelling for 3 seconds at each voltage. In the first minute of operation (left panel) the device current and EQE falls dramatically, following what was similarly observed qualitatively for brightness. At longer times and as the voltage continues to increase (right panel) the current increases again, but never reaches its initial level. The EQE does not recover at all. Note that this measurement does not display the dramatic decrease in brightness over the first 3 seconds, as this emission is averaged into the first data point.

S6 X-ray Crystallographic data

General X-ray Crystallography experimental details

X-ray diffraction experiments (**Table S3**) were carried out for **3** on a Bruker 3-circle D8 Venture diffractometer with a Photon100 CMOS detector, for **4** on an Xcalibur 4-circle κ -diffractometer with Sapphire3 CCD area detector, using Mo- $K\alpha$ radiation ($\lambda = 0.71073 \text{ \AA}$) from a $I\mu\text{S}$ -microsource with focusing mirrors (**3**) or an Enhance source with graphite monochromator (**4**). Structure **3** was solved by direct methods using SHELXS 2013/1 program,¹² **4** by dual-space intrinsic phasing method using SHELXT 2018/2 program.¹³ Both structures were refined using SHELXL 2018/3¹⁴ software on OLEX2 platform.¹⁵ Structure **4** contains one DCM molecule of crystallisation per asymmetric unit, as well as an isolated triangular void of ca. 250 \AA^3 lying astride a twofold axis and presumably containing a chaotically disordered DCM molecule (i.e. half of a molecule per asymmetric unit), which was masked using PLATON SQUEEZE procedure.¹⁶

Table S3. Crystal data and experimental details

Compound	3	4
CCDC	1887606	1887607
Formula	C ₄₃ H ₃₀ F ₆ N ₂ O ₆ S	C ₄₉ H ₃₀ F ₁₈ N ₂ O ₂ S·3/2 CH ₂ Cl ₂
Formula Weight	816.75	1180.20
<i>T</i> /K	120	120
Crystal System	triclinic	monoclinic
Space Group	<i>P</i> $\bar{1}$ (no. 2)	<i>C</i> 2/ <i>c</i> (no. 15)
<i>a</i> /Å	7.3762(4)	30.4672(11)
<i>b</i> /Å	26.4048(15)	14.1023(3)
<i>c</i> /Å	27.4985(15)	24.3625(8)
α /°	98.350(2)	90
β /°	93.841(2)	105.687(4)
γ /°	91.895(2)	90
<i>V</i> /Å ³	5282.2(5)	10077.6(6)
<i>Z</i>	6	8
<i>D</i> _{calc.} / g cm ⁻³	1.541	1.556
μ /mm ⁻¹	0.18	0.33
2 θ _{max} /°	55	50
Measured Refls.	94153	34211
Independent Refls.	24224	8849
with <i>I</i> > 2 σ (<i>I</i>)	16827	7217
<i>R</i> _{int}	0.051	0.034
Parameters/ restraints	1591/0	706/15
$\Delta\rho$ /eÅ ⁻³	0.5, -0.49	0.42, -0.37
Goodness of fit	1.018	1.028
<i>R</i> ₁ , <i>wR</i> ₂ (all data)	0.088, 0.151	0.054, 0.107
<i>R</i> ₁ , <i>wR</i> ₂ [<i>I</i> > 2 σ (<i>I</i>)]	0.054, 0.135	0.042, 0.100

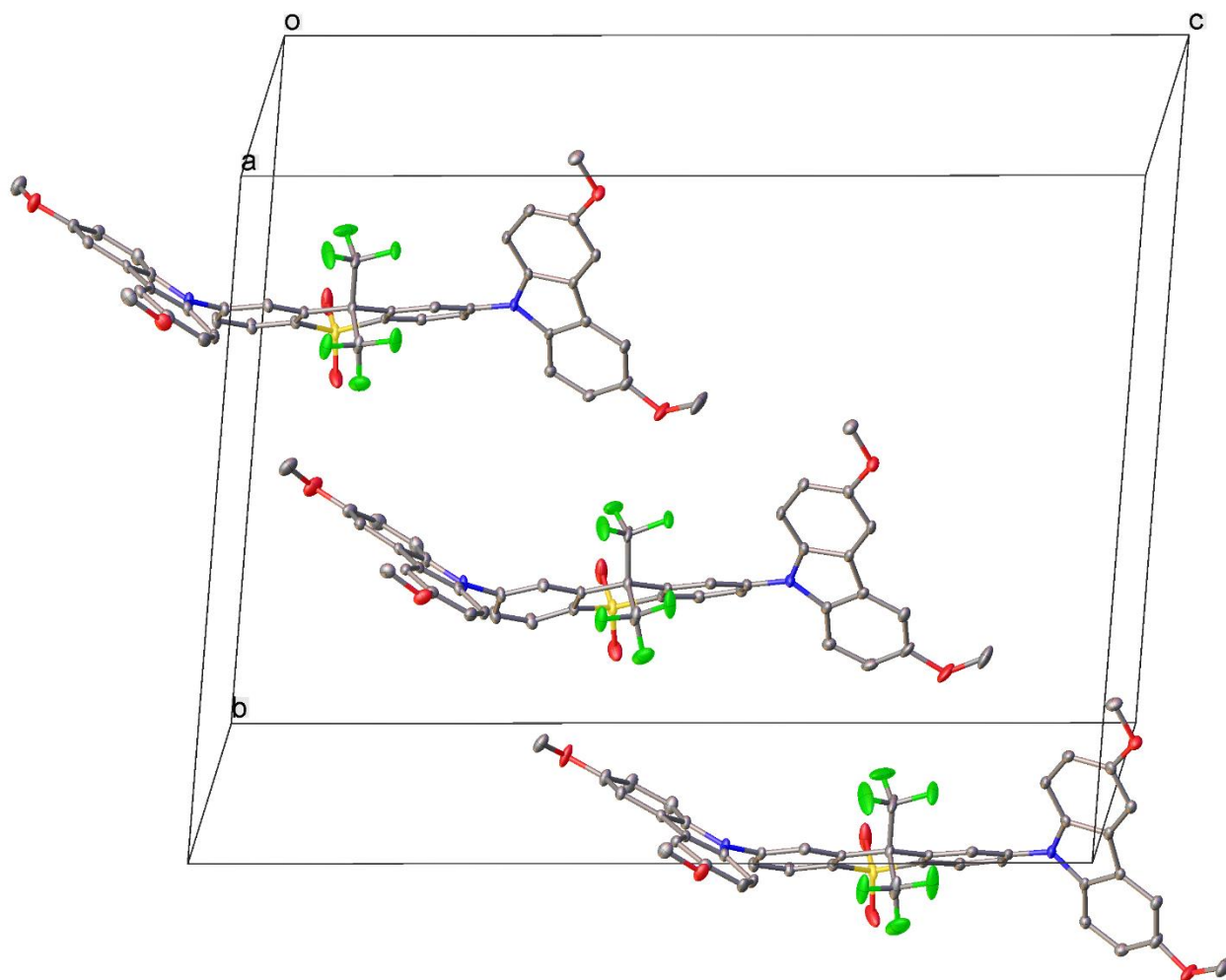


Figure S6a Three independent molecules in the unit cell of the crystal structure of **3**. Atomic displacement ellipsoids are drawn at the 50% probability level, H atoms are omitted.

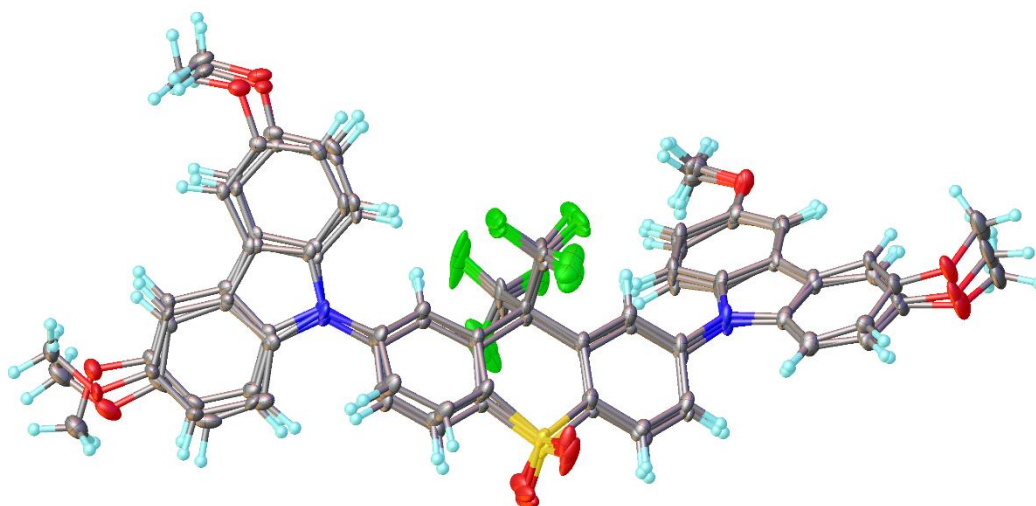


Figure S6b Overlay of the independent molecules of **3** with rmsd misfit values on all atoms of 0.533-0.602 Å between these geometries.

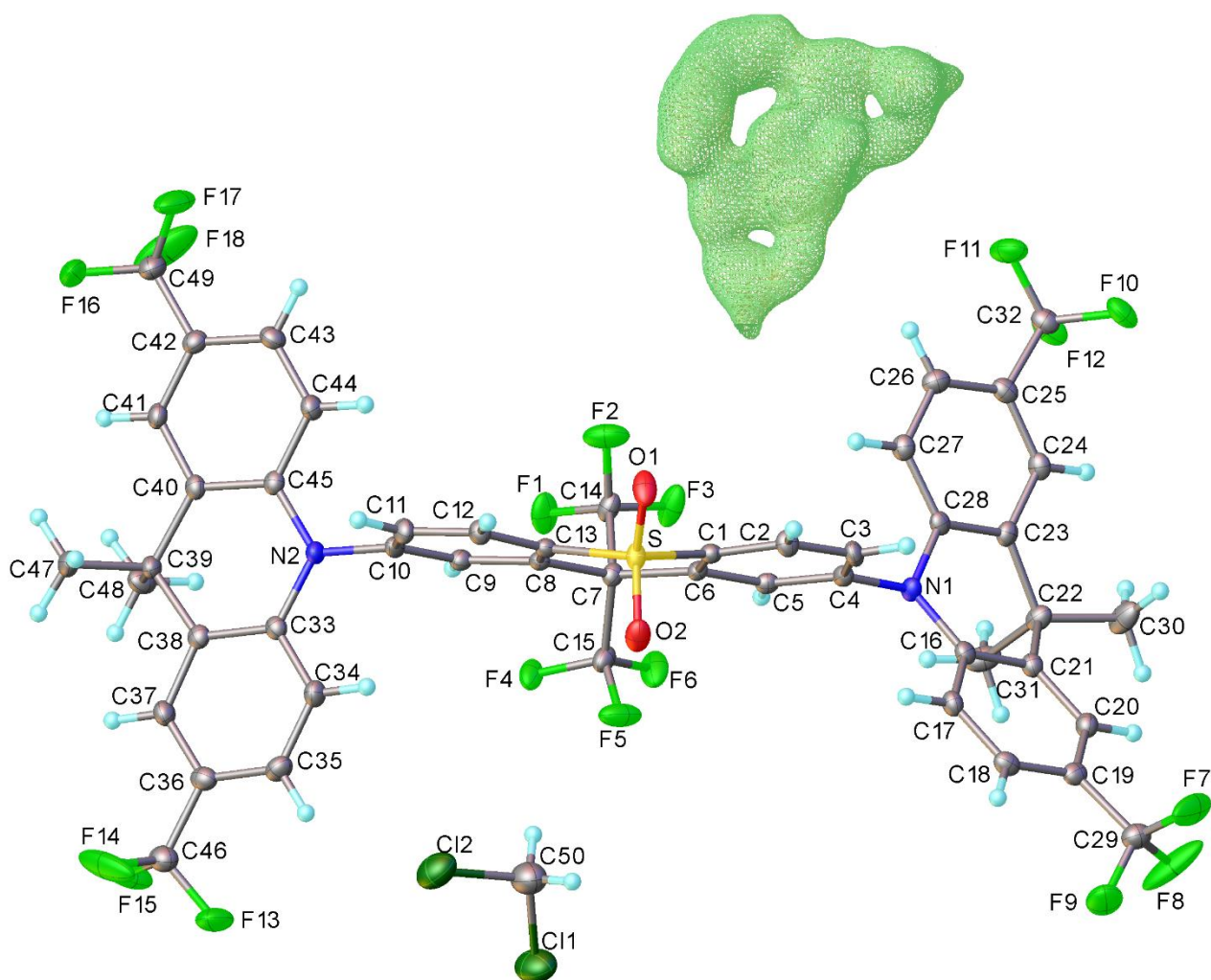


Figure S6c The asymmetric unit in the structure of $4 \frac{3}{2} \text{CH}_2\text{Cl}_2$. Green contours indicate the electron density of the disordered CH_2Cl_2 molecule, lying astride a crystallographic twofold axis. Minor disorder of the Cl(1) and C(49)F₃ is omitted

S7 Computational data

All geometry optimizations were carried out with the Gaussian 09 package.¹⁷ Ground state (S_0) and excited triplet state (T_1) geometries were fully optimized from different starting geometries without symmetry constraints using the Coulomb-attenuating method (CAM) CAM-B3LYP¹⁸ with the 6-31(d) basis set.^{19,20} The CAM-B3LYP functional has been successfully applied to similar TADF molecules elsewhere.²¹ The popular B3LYP^{22, 23} functional (and indeed many other pure/hybrid density functional theory (DFT) methods with zero/low Hartree-Fock (HF) wave contributions) is known to significantly underestimate charge transfer (CT) energies with respect to local excitation (LE) energies.²⁴ All fully optimized S_0 geometries were found to be true minima based on no imaginary frequencies found from frequency calculations. The constrained geometries were partially optimised using the `opt=modredundant` command. The optimizations of the open shell excited triplet state (T_1) geometries were determined by unrestricted DFT (UDFT) with charge and multiplicity at 0 and 3 respectively. The same optimized triplet state (T_1) geometries can be obtained using the `td opt` command (TD-DFT) but the UDFT method is much quicker.

Singlet excited state (S_1) geometries were optimized using the `td opt` command (TD-DFT) from fully optimized S_0 geometries as starting geometries at CAM-B3LYP/6-31G(d) with the Gaussian 16 package.²⁵ The larger HF contribution in CAM-B3LYP means that all computed transition energies are generally overestimated in time-dependent density functional theory (TD-DFT) calculations at CAM-B3LYP. The parameter μ in CAM-B3LYP determines the balance of DFT to HF exchange at the intermediate point in the long-range exchange interaction.¹⁸ If $\mu = 0$, the long-range-corrected (LC) DFT calculation²⁶ corresponds to the pure (non-LC) DFT calculation, and conversely $\mu = \infty$ corresponds to the standard HF calculation. The parameter μ in CAM-B3LYP is 0.33 and, to lower the HF contribution, this parameter is adjusted to 0.27 for TD-DFT computations here for direct comparison with experimental emission data (Table S4). The correction factor was determined by using a mean absolute error (MAE) method between experimental and computed frequencies. An absolute error means the modulus of the difference between the computed and observed values and the absolute errors are averaged to give the MAE value. The lower the MAE value the better the correction factor used. We are then able to obtain realistic predicted values from DFT computations for comparison with experimental data.

The six lowest singlet and six lowest triplet transitions were predicted from TD-DFT computations on the optimised S_1 and T_1 geometries. The predicted absorption spectra were produced visually from 25 lowest singlet states determined by TD-DFT. No oscillator strengths could be obtained for triplet state transitions within the TD-DFT setup in the Gaussian software. Natural transition orbital (NTO) calculations were performed on the optimised S_1 to visualize the hole and particle orbitals. The NTO figures were generated using the Gabedit package.²⁷ The %CT values were obtained by i) defining the atoms for donor and acceptor units, ii) calculating the %donor and %acceptor values in each molecular orbital using electronic structure calculations and iii) calculating the %CT from NTO orbitals using the TD-DFT generated data and the %donor and %acceptor values with GaussSum software.²⁸ Spin-orbit coupling matrix elements (SOCME) were calculated using the Orca package (Table S9).²⁹

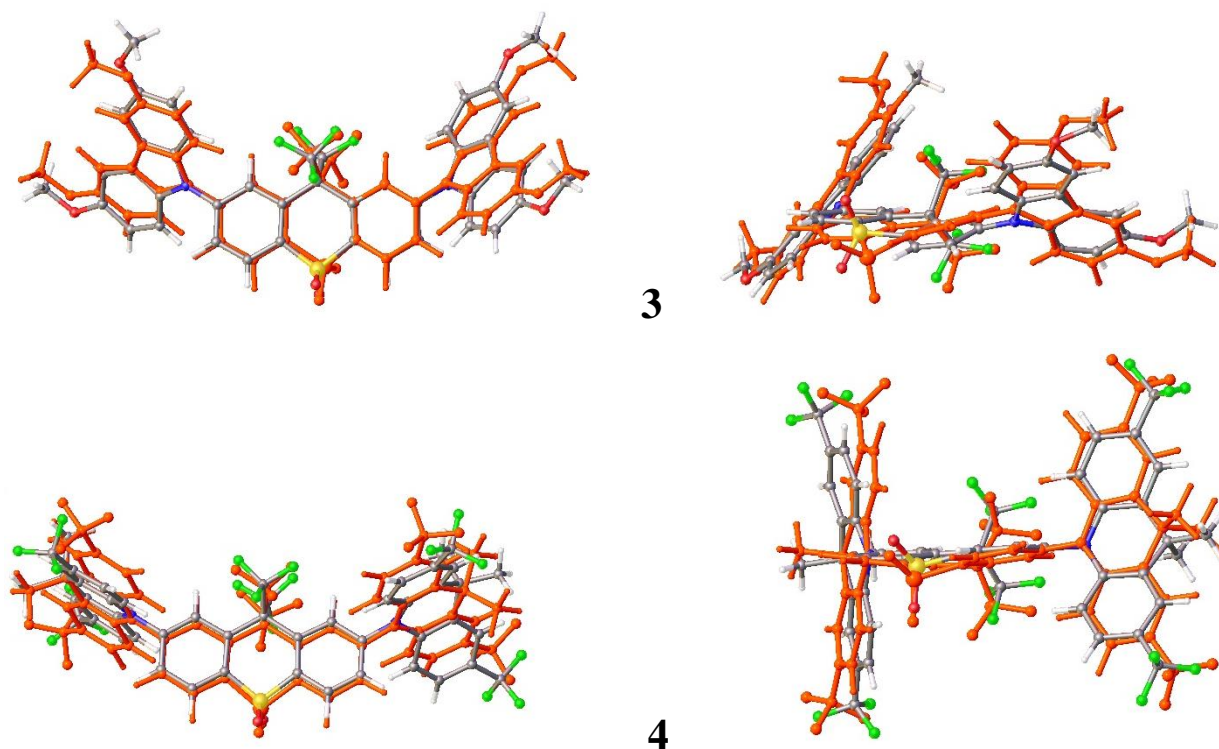


Figure S7a. X-ray geometries of **3** (top) and **4** overlaid with their corresponding optimized S_0 geometries in orange [with root mean square distance (rmsd) misfit values on all atoms of 0.854 Å for **3** and 0.945 Å for **4**].

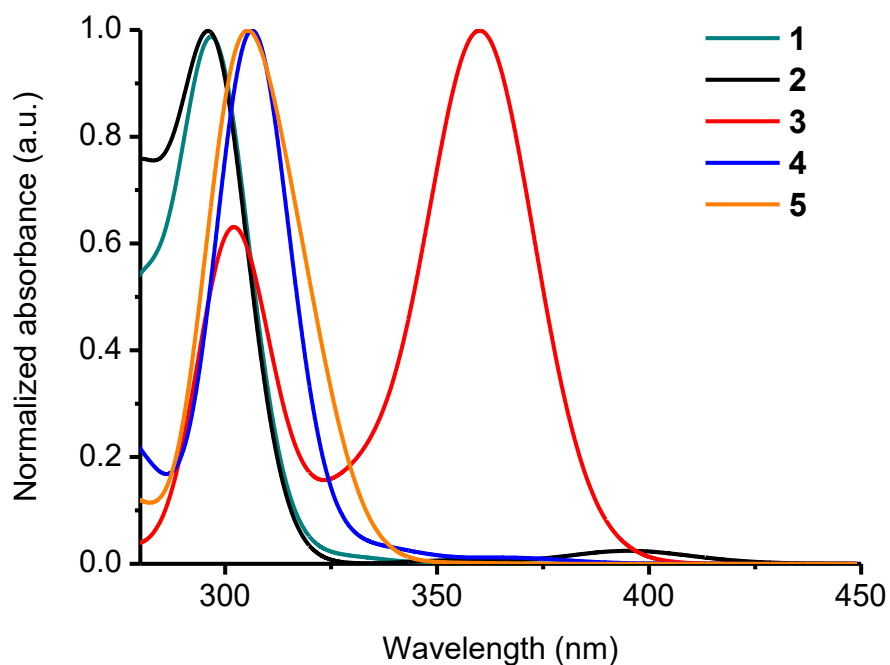


Figure S7b. Simulated absorption spectra with scaling factor of 1.12 and bands with fixed gaussian peak height peak width (phpw) of 0.15 eV. Only singlet state transitions have calculated oscillator strengths from TD-DFT computations on S_0 optimized geometries.

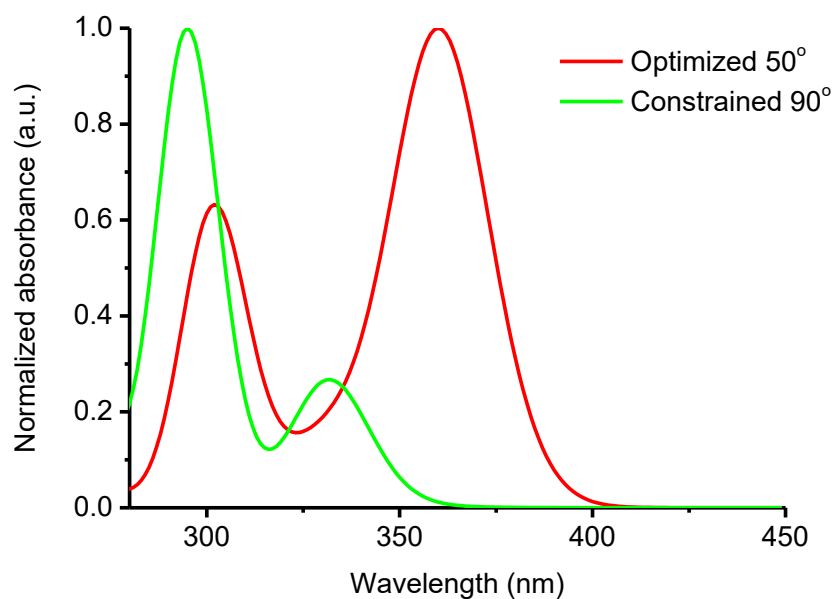


Figure S7c. Simulated absorption spectra for **3** at different D-A orientations. Lowest singlet state transition oscillator strengths, 0.6726 for optimized geometry and 0.0003 for constrained 90° geometry.

Table S4. Determination of the parameter μ in CAM-B3LYP for direct comparison with experimental emission data of $S_1(\text{CT})$ in eV by use of mean absolute error (MAE) values. The lowest MAE value was found for $\mu = 0.27$.

	μ	1	2	3	4	5	MAE
Experimental		3.00	2.77	2.81	3.05	3.30	
CAM-B3LYP	0.33	3.24	2.89	3.00	3.13	3.44	0.152
	0.30	3.18	2.83	2.94	3.07	3.38	0.091
	0.27	3.11	2.74	2.86	3.00	3.31	0.050
	0.25	3.06	2.70	2.80	2.94	3.25	0.056
	0.20	2.90	2.55	2.63	2.79	3.07	0.198
B3LYP	-	2.36	1.99	1.96	2.24	2.57	0.761

Table S5. TDDFT data on optimized and partially-optimized geometries of **3**.

Fully optimised	Energy eV	State	Nature	%CT	Constrained	Energy eV	State	Nature	%CT
S ₀ (50,50)	3.08	T ₁	³ D	13	S ₀ (90,90)	3.10	T ₁	³ D	0
	3.08	T ₂	³ D	7		3.10	T ₂	³ D	0
	3.87	S ₁	¹ CT	82		3.69	S ₁	¹ CT	95
	3.99	S ₂	¹ CT	85		3.71	S ₂	¹ CT	95
ΔE_{ST}	0.81				ΔE_{ST}	0.59			
S ₁ (90,50)	2.84	T ₁	³ CT	95	S ₁ (50,50)	2.61	T ₁	³ CT	67
	2.86	S ₁	¹ CT	95		3.08	T ₂	³ D	9
	2.89	T ₂	³ A	29		3.30	S ₁	¹ CT	86
	3.68	S ₂	¹ CT	97		3.90	S ₂	¹ CT	85
ΔE_{ST}	0.02				ΔE_{ST}	0.69			

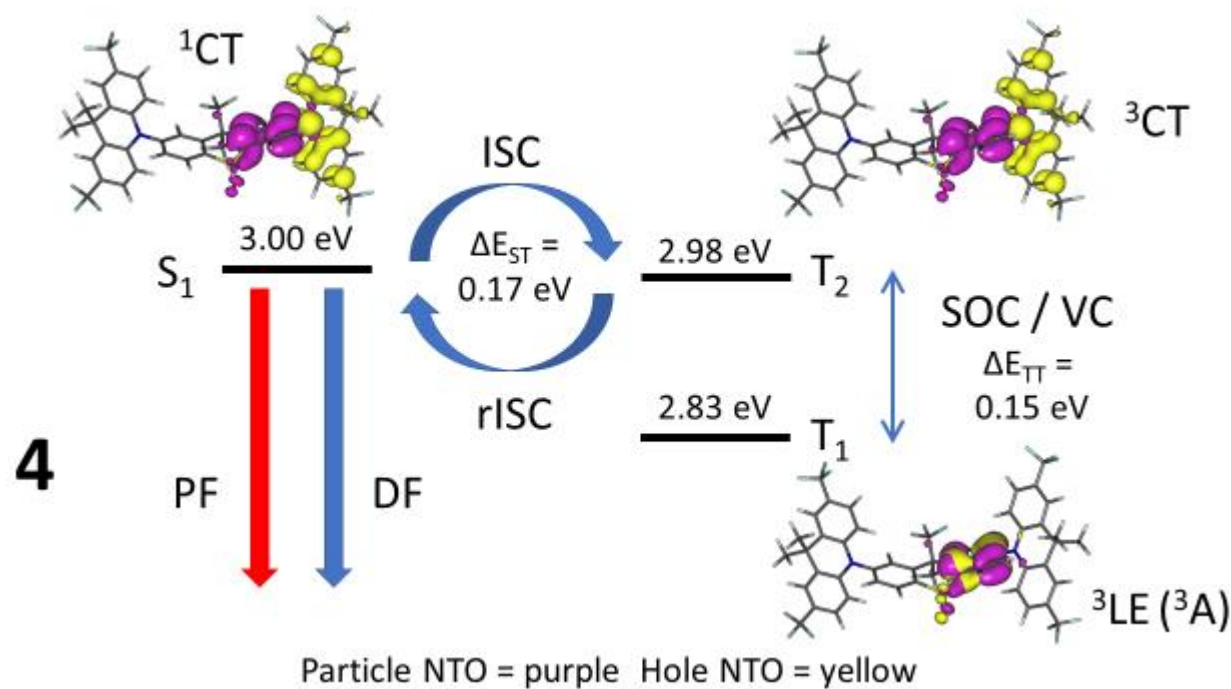
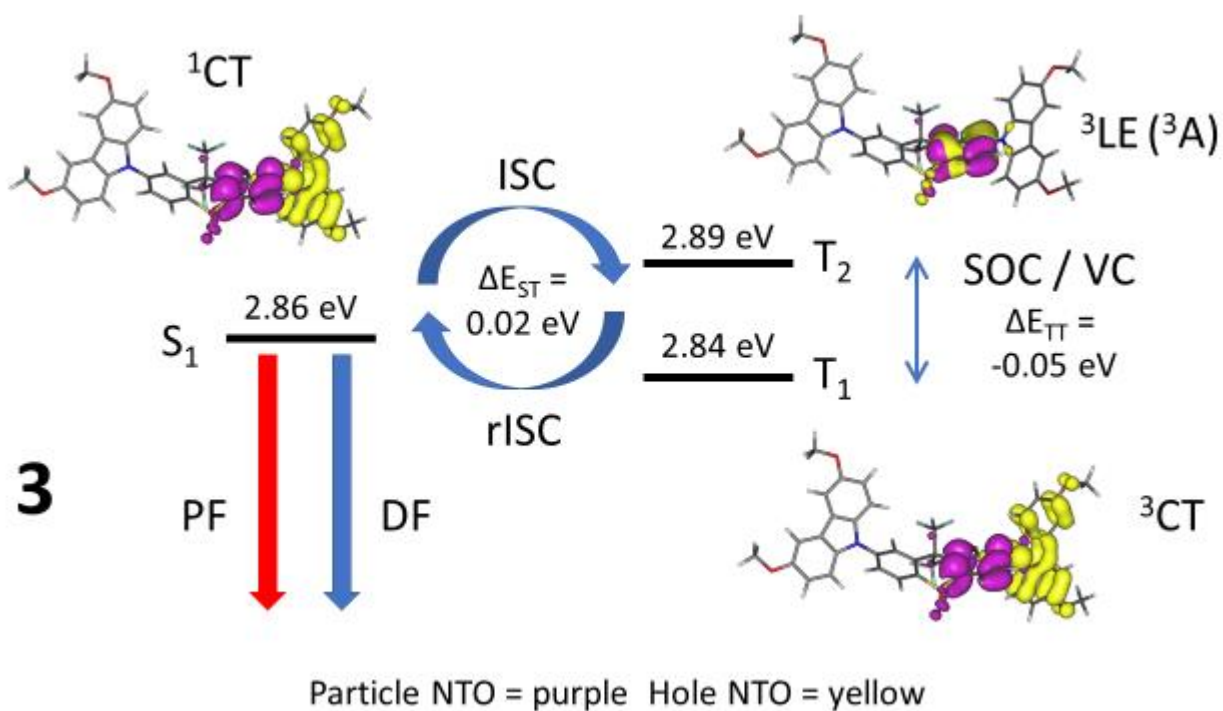


Figure S7d. Energy diagrams illustrating TADF in **3** and **4** with natural transition orbitals for each state on optimized S_1 excited state geometries from TD-DFT computations. PF = prompt fluorescence, DF = (thermally activated) delayed fluorescence, ISC = intersystem crossing, rISC = reverse intersystem crossing, SOC = spin orbit coupling, VC = vibronic coupling, $\Delta E_{ST} = S_1$ energy - T_1 energy, $\Delta E_{TT} = {}^3CT$ energy - 3LE energy, 1CT = singlet charge transfer state, 3CT = triplet charge transfer state, 3LE = local triplet excitation state, 3A = local triplet excitation at the acceptor unit.

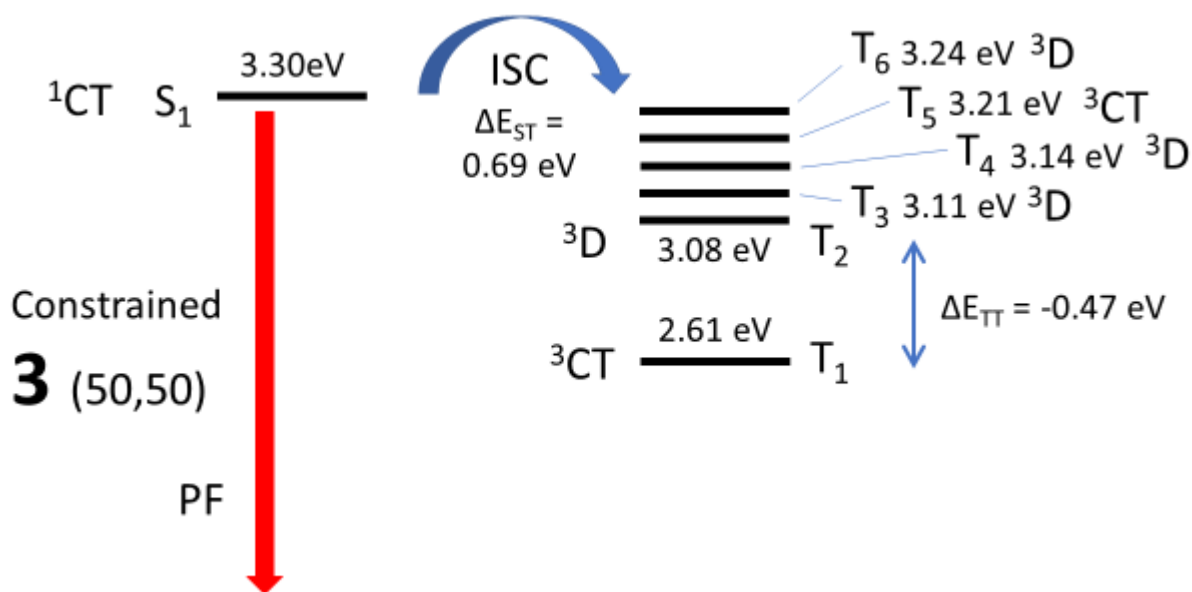


Figure S7e. Energy diagram showing lowest excited states on the optimized S_1 excited state geometry of **3** with constrained D-A dihedral angles of 50° from TD-DFT computations. PF = prompt fluorescence, ISC = intersystem crossing, $\Delta E_{ST} = S_1$ energy - T_1 energy, $\Delta_{TT} = {}^3CT$ energy - 3LE energy, 1CT = singlet charge transfer state, 3CT = triplet charge transfer state, 3LE = local triplet excitation state, 3A = local triplet excitation at the acceptor unit, 3D = local triplet excitation at the donor unit.

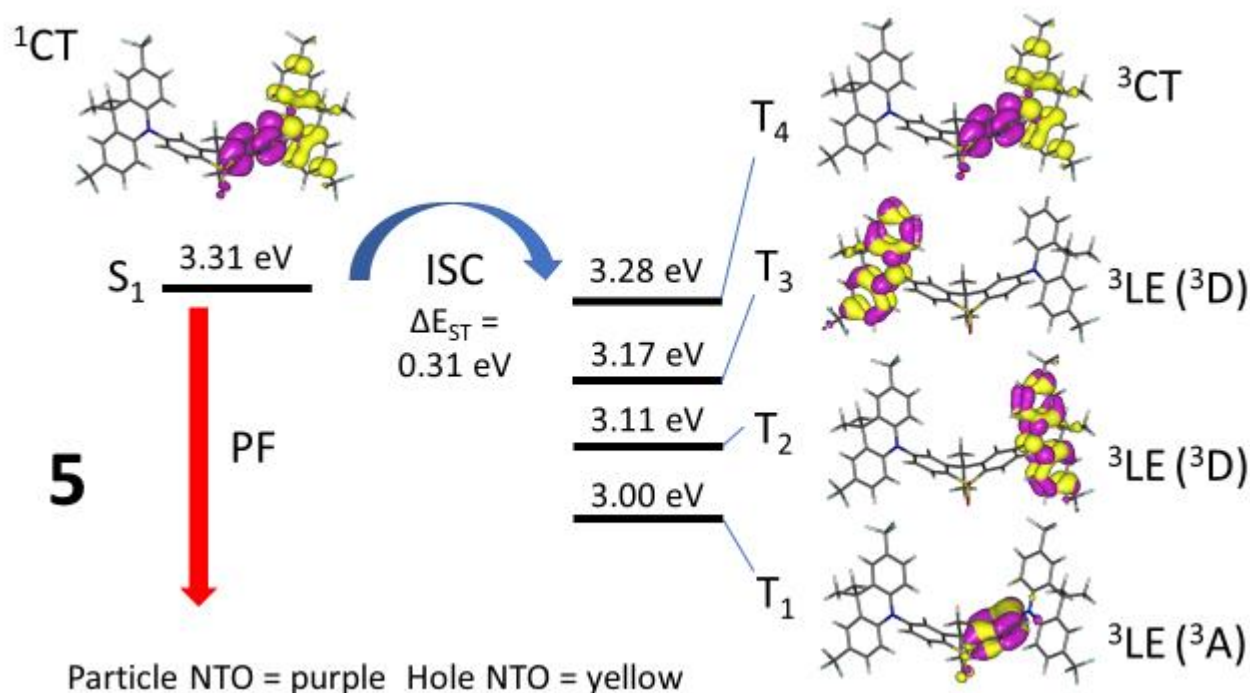


Figure S7f. Energy diagram reflecting absence of TADF in **5** with natural transition orbitals for each state on the optimized S_1 excited state geometry from TD-DFT computations. PF = prompt fluorescence, ISC = intersystem crossing, $\Delta E_{ST} = S_1$ energy - T_1 energy, 1CT = singlet charge transfer state, 3CT = triplet charge transfer state, 3LE = local triplet excitation state, 3A = local triplet excitation at the acceptor unit, 3D = local triplet excitation at the donor unit.

Table S6. TDDFT data on optimized S_0 geometries of **1–5**.

	Energy eV	State	Nature	%CT
1	3.27	T ₁	³ D	4
	3.27	T ₂	³ D	4
	3.70	S ₁	¹ CT	94
	3.71	S ₂	¹ CT	88
	ΔE_{ST} 0.43			
2	3.27	T ₁	³ D	0
	3.27	T ₂	³ D	0
	3.51	S ₁	¹ CT	94
	3.55	S ₂	¹ CT	94
	ΔE_{ST} 0.24			
3	3.08	T ₁	³ D	13
	3.08	T ₂	³ D	7
	3.87	S ₁	¹ CT	82
	3.99	S ₂	¹ CT	85
	ΔE_{ST} 0.81			
4	3.19	T ₁	³ D	5
	3.19	T ₂	³ D	4
	3.78	S ₁	¹ CT	84
	3.81	S ₂	¹ CT	85
	ΔE_{ST} 0.59			
5	3.18	T ₁	³ D	20
	3.18	T ₂	³ D	20
	3.97	S ₁	¹ CT	92
	3.97	S ₂	¹ CT	92
	ΔE_{ST} 0.79			

Table S7. TDDFT data on optimized T₁ geometries of **1–5**.

	Energy eV	State	Nature	%CT
1	2.43	T ₁	³ CT	67
	3.23	T ₂	³ D	4
	3.27	S ₁	¹ CT	80
	3.70	S ₂	¹ CT	90
ΔE_{ST}	0.80			
2	2.13	T ₁	³ CT	57
	2.92	S ₁	¹ CT	83
	3.21	T ₂	³ D	21
	3.57	S ₂	¹ CT	92
ΔE_{ST}	0.79			
3	2.06	T ₁	³ CT	55
	3.08	T ₂	³ D	28
	3.22	S ₁	¹ CT	78
	3.87	S ₂	¹ CT	80
ΔE_{ST}	1.16			
4	2.01	T ₁	³ CT	45
	3.05	S ₁	¹ CT	59
	3.18	T ₂	³ D	2
	3.82	S ₂	¹ CT	80
ΔE_{ST}	1.04			
5	2.42	T ₁	³ CT	67
	3.17	T ₂	³ D	10
	3.42	S ₁	¹ CT	77
	3.96	S ₂	¹ CT	88
ΔE_{ST}	1.00			

Table S8. TDDFT data on optimized S_1 geometries of **1-5** with experimental emission data for comparison. %CT represents the % transfer of density from the particle natural transition orbital (NTO) to the hole NTO. $\Delta E_{ST} = S_1$ energy – T_1 energy, $\Delta E_{TT} = {}^3CT$ energy – 3LE energy. 3A is triplet local excitation at the acceptor unit, 3D is triplet local excitation at the donor unit.

	Energy eV	State	Nature	%CT	S_1 (exp) eV	T_1 (exp) eV	ΔE_{ST} (exp) eV		
1	3.04	T_1	3A	12	3.08	3.01	0.07		
	3.09	T_2	3CT	86					
	3.11	S_1	1CT	94					
	3.65	S_2	1CT	93					
	ΔE_{ST}	0.07							
	ΔE_{TT}	0.05							
2	2.74	T_1	3CT	95	2.86	2.78	0.08		
	2.76	S_1	1CT	95					
	2.84	T_2	3A	5					
	3.52	S_2	1CT	94					
	ΔE_{ST}	0.02							
	ΔE_{TT}	-0.10							
3	2.84	T_1	3CT	95	2.93	2.71	0.22		
	2.86	S_1	1CT	95					
	2.89	T_2	3A	29					
	3.68	S_2	1CT	97					
	ΔE_{ST}	0.02							
	ΔE_{TT}	-0.05							
4	2.83	T_1	3A	6	3.14	2.92	0.22		
	2.98	T_2	3CT	74					
	3.00	S_1	1CT	74					
	3.80	S_2	1CT	82					
	ΔE_{ST}	0.17							
	ΔE_{TT}	0.15							
5	3.00	T_1	3A	17	3.42	3.07	0.35		
	3.11	T_2	3D	20					
	3.31	S_1	1CT	93					
	3.92	S_2	1CT	92					
	ΔE_{ST}	0.31							
	ΔE_{TT}	0.11							

Table S9. Calculated spin orbit coupling matrix elements (SOCME), $\langle S_1 | \hat{H}_{so} | T_1 \rangle$ and $\langle S_1 | \hat{H}_{so} | T_2 \rangle$ in cm^{-1} for optimized S_1 geometries of **1-5**.

	$\langle S_1 \hat{H}_{so} T_1 \rangle$ cm^{-1}	Nature of T_1	%CT of T_1	$\langle S_1 \hat{H}_{so} T_2 \rangle$ cm^{-1}	Nature of T_2	%CT of T_2
1	1.37	3A	12	0.12	3CT	86
2	0.04	3CT	95	1.30	3A	5
3	0.04	3CT	95	1.41	3A	29
4	1.30	3A	6	0.17	3CT	74
5	1.45	3A	17	0.77	3D	20

S8 References

- G. R. Fulmer, A. J. M. Miller, N. H. Sherden, H. E. Gottlieb, A. Nudelman, B. M. Stoltz, J. E. Bercaw and K. I. Goldberg, NMR Chemical Shifts of Trace Impurities: Common Laboratory Solvents, Organics, and Gases in Deuterated Solvents Relevant to the Organometallic Chemist, *Organometallics*, 2010, **29**, 2176-2179.
- P. L. dos Santos, J. S. Ward, M. R. Bryce and A. P. Monkman, Using Guest-Host Interactions To Optimize the Efficiency of TADF OLEDs, *J. Phys. Chem. Lett.*, 2016, **7**, 3341-3346.
- S. N. Bagriantsev, K. H. Ang, A. Gallardo-Godoy, K. A. Clark, M. R. Arkin, A. R. Renslo and D. L. Minor, A High-Throughput Functional Screen Identifies Small Molecule Regulators of Temperature- and Mechano-Sensitive K-2P Channels, *ACS Chem. Biol.*, 2013, **8**, 1841-1851.
- P. L. Santos, J. S. Ward, P. Data, A. S. Batsanov, M. R. Bryce, F. B. Dias and A. P. Monkman, Engineering the singlet-triplet energy splitting in a TADF molecule, *J. Mater. Chem. C*, 2016, **4**, 3815-3824.
- M.-L. Louillat and F. W. Patureau, Toward Polynuclear Ru–Cu Catalytic Dehydrogenative C–N Bond Formation, on the Reactivity of Carbazoles, *Org. Lett.*, 2013, **15**, 164-167.
- S. Scholer, K. Merz, A. Puls, M. Winter and G. Dyker, Synthesis and Characterization of ortho-Thio-Functionalized Triarylmethyl Palladium Complexes, *Eur. J. Inorg. Chem.*, 2015, 53-57.
- A. Lerchen, T. Knecht, M. Koy, C. G. Daniliuc and F. Glorius, A General $Cp^*Co(III)$ -Catalyzed Intramolecular C–H Activation Approach for the Efficient Total Syntheses of Aromathecine, Protoberberine, and Tylophora Alkaloids, *Chem. Eur. J.*, 2017, **23**, 12149-12152.
- T. Vlaar, P. Mampuy, M. Helliwell, B. U. Maes, R. V. Orru and E. Ruijter, Multicomponent synthesis of 4-aminophthalazin-1(2H)-ones by palladium-catalyzed isocyanide insertion, *J. Org. Chem.*, 2013, **78**, 6735-6745.
- L. Mahendar and G. Satyanarayana, Copper catalyzed coupling of protecting group free and sterically hindered 2-bromobenzyl tertiary alcohols with phenols and anilines: facile synthesis of xanthenes and dihydroacridines, *RSC Adv.*, 2016, **6**, 20588-20597.
- C. Rothe and A. P. Monkman, Triplet exciton migration in a conjugated polyfluorene, *Phys. Rev. B*, 2003, **68**, 075208.
- J. S. Moon, D. H. Ahn, S. W. Kim, S. Y. Lee, J. Y. Lee and J. H. Kwon, delta-Carboline-based bipolar host materials for deep blue thermally activated delayed fluorescence OLEDs with high efficiency and low roll-off characteristic, *RSC Adv.*, 2018, **8**, 17025-17033.
- G. M. Sheldrick, A short history of SHELX, *Acta Crystallogr. A*, 2008, **64**, 112-122.
- G. M. Sheldrick, SHELXT - integrated space-group and crystal-structure determination, *Acta Crystallogr. A*, 2015, **71**, 3-8.

14. G. M. Sheldrick, Crystal structure refinement with SHELXL, *Acta Crystallogr. C Struct. Chem.*, 2015, **71**, 3-8.
15. O. V. Dolomanov, L. J. Bourhis, R. J. Gildea, J. A. K. Howard and H. Puschmann, OLEX2: a complete structure solution, refinement and analysis program, *J. Appl. Crystallogr.*, 2009, **42**, 339-341.
16. A. L. Spek, PLATON SQUEEZE: a tool for the calculation of the disordered solvent contribution to the calculated structure factors, *Acta Crystallogr. C Struct. Chem.*, 2015, **71**, 9-18.
17. M. J. Frisch, G. W. Trucks, H. B. Schlegel, G. E. Scuseria, M. A. Robb, J. R. Cheeseman, G. Scalmani, V. Barone, B. Mennucci, G. A. Petersson, H. Nakatsuji, M. Caricato, X. Li, H. P. Hratchian, A. F. Izmaylov, J. Bloino, G. Zheng, J. L. Sonnenberg, M. Hada, M. Ehara, K. Toyota, R. Fukuda, J. Hasegawa, M. Ishida, T. Nakajima, Y. Honda, O. Kitao, H. Nakai, T. Vreven, J. A. Montgomery, Jr.; , J. E. Peralta, F. Ogliaro, M. Bearpark, J. J. Heyd, E. Brothers, K. N. Kudin, V. N. Staroverov, R. Kobayashi, J. Normand, K. Raghavachari, A. Rendell, J. C. Burant, S. S. Iyengar, J. Tomasi, M. Cossi, N. Rega, J. M. Millam, M. Klene, J. E. Knox, J. B. Cross, V. Bakken, C. Adamo, J. Jaramillo, R. Gomperts, R. E. Stratmann, O. Yazyev, A. J. Austin, R. Cammi, C. Pomelli, J. W. Ochterski, R. L. Martin, K. Morokuma, V. G. Zakrzewski, G. A. Voth, P. Salvador, J. J. Dannenberg, S. Dapprich, A. D. Daniels, Ö. Farkas, J. B. Foresman, J. V. Ortiz, J. Cioslowski and D. J. Fox, Gaussian 09, Revision A.02, *Gaussian, Inc Wallingford CT*, 2009.
18. T. Yanai, D. P. Tew and N. C. Handy, A new hybrid exchange-correlation functional using the Coulomb-attenuating method (CAM-B3LYP), *Chem. Phys. Lett.*, 2004, **393**, 51-57.
19. G. A. Petersson, A. Bennett, T. G. Tensfeldt, M. A. Allaham, W. A. Shirley and J. Mantzaris, A Complete Basis Set Model Chemistry .1. The Total Energies of Closed-Shell Atoms and Hydrides of the 1st-Row Elements, *J. Chem. Phys.*, 1988, **89**, 2193-2218.
20. G. A. Petersson and M. A. Al Laham, A Complete Basis Set Model Chemistry .2. Open-Shell Systems and the Total Energies of the 1st-Row Atoms, *J. Chem. Phys.*, 1991, **94**, 6081-6090.
21. P. K. Samanta, D. Kim, V. Coropceanu and J. L. Bredas, Up-Conversion Intersystem Crossing Rates in Organic Emitters for Thermally Activated Delayed Fluorescence: Impact of the Nature of Singlet vs Triplet Excited States, *J. Am. Chem. Soc.*, 2017, **139**, 4042-4051.
22. A. D. Becke, Density-Functional Thermochemistry .3. The Role of Exact Exchange, *J. Chem. Phys.*, 1993, **98**, 5648-5652.
23. C. T. Lee, W. T. Yang and R. G. Parr, Development of the Colle-Salvetti Correlation-Energy Formula into a Functional of the Electron-Density, *Phys. Rev. B*, 1988, **37**, 785-789.
24. A. Dreuw, J. L. Weisman and M. Head-Gordon, Long-range charge-transfer excited states in time-dependent density functional theory require non-local exchange, *J. Chem. Phys.*, 2003, **119**, 2943-2946.
25. M. J. Frisch, G. W. Trucks, H. B. Schlegel, G. E. Scuseria, M. A. Robb, J. R. Cheeseman, G. Scalmani, V. Barone, G. A. Petersson, H. Nakatsuji, X. Li, M. Caricato, A. V. Marenich, J. Bloino, B. G. Janesko, R. Gomperts, B. Mennucci, H. P. Hratchian, J. V. Ortiz, A. F. Izmaylov, J. L. Sonnenberg, D. Williams-Young, F. Ding, F. Lipparini, F. Egidi, J. Goings, B. Peng, A. Petrone, T. Henderson, D. Ranasinghe, V. G. Zakrzewski, J. Gao, N. Rega, G. Zheng, W. Liang, M. Hada, M. Ehara, K. Toyota, R. Fukuda, J. Hasegawa, M. Ishida, T. Nakajima, Y. Honda, O. Kitao, H. Nakai, T. Vreven, K. Throssell, J. A. Montgomery, Jr., J. E. Peralta, F. Ogliaro, M. J. Bearpark, J. J. Heyd, E. N. Brothers, K. N. Kudin, V. N. Staroverov, T. A. Keith, R. Kobayashi, J. Normand, K. Raghavachari, A. P. Rendell, J. C. Burant, S. S. Iyengar, J. Tomasi, M. Cossi, J. M. Millam, M. Klene, C. Adamo, R. Cammi, J. W. Ochterski, R. L. Martin, K. Morokuma, O. Farkas, J. B. Foresman, and D. J. Fox, Gaussian 16, Revision B.01, *Gaussian, Inc., Wallingford CT*, 2016.
26. Y. Tawada, T. Tsuneda, S. Yanagisawa, T. Yanai and K. Hirao, A long-range-corrected time-dependent density functional theory, *J. Chem. Phys.*, 2004, **120**, 8425-8433.
27. A. R. Allouche, Gabedit-A Graphical User Interface for Computational Chemistry Softwares, *J. Comput. Chem.*, 2011, **32**, 174-182.

28. N. M. O'Boyle, A. L. Tenderholt and K. M. Langner, cclib: A library for package-independent computational chemistry algorithms, *J. Comput. Chem.*, 2008, **29**, 839-845.
29. F. Neese, D. Aravena, M. Atanasov, A. A. Auer, U. Becker, G. Bistoni, M. Brehm, D. Bykov, V. G. Chilkuri, D. Datta, A. K. Dutta, D. Ganyushin, M. Garcia, Y. Guo, A. Hansen, B. Helmich-Paris, L. Huntington, R. Izsak, C. Kollmar, S. Kossmann, M. Krupicka, L. Lang, D. Lenk, D. Liakos, D. Manganas, D. Pantazis, T. Petrenko, P. Pinski, C. Reimann, M. Retegan, C. Riplinger, T. Risthaus, M. Roemelt, M. Saitow, B. Sandhofer, A. Sen, K. Sivalingam, B. de Souza, G. Stoychev, W. Van den Heuvel, B. Wezislá and F. Wennmohs, Orca version 4.1.1., *Department of Theory and Spectroscopy, Max Planck Institute fuer Kohlenforschung, Kaiser Wilhelm Platz 1, D-45470 Muelheim/Ruhr, Germany*. 2019.